Advances in Colloid and Interface Science 288 (2021) 102336

Contents lists available at ScienceDirect

Advances in Colloid and Interface Science

journal homepage: www.elsevier.com/locate/cis

Historical Perspective

Hydrodynamics and surface properties influence biofilm proliferation

Milos Krsmanovic [a], Dipankar Biswas [a], Hessein Ali [a], Aloke Kumar [b], Ranajay Ghosh [a], Andrew K. Dickerson [a,*]

[a] Department of Mechanical and Aerospace Engineering, University of Central Florida, USA
[b] Department of Mechanical Engineering, Indian Institute of Science, Bangalore, India

ARTICLE INFO

Article history:
2 December 2020
Available online 10 December 2020

Keywords:
Cell motility
Shear stress
Biofilm structure
Surface pattern
Surface energy

ABSTRACT

A biofilm is an interface-associated colloidal dispersion of bacterial cells and excreted polymers in which microorganisms find protection from their environment. Successful colonization of a surface by a bacterial community is typically a detriment to human health and property. Insight into the biofilm life-cycle provides clues on how their proliferation can be suppressed. In this review, we follow a cell through the cycle of attachment, growth, and departure from a colony. Among the abundance of factors that guide the three phases, we focus on hydrodynamics and stratum properties due to the synergistic effect such properties have on bacteria rejection and removal. Cell motion, whether facilitated by the environment via medium flow or self-actuated by use of an appendage, drastically improves the survivability of a bacterium. Once in the vicinity of a stratum, a single cell is exposed to near-surface interactions, such as van der Waals, electrostatic and specific interactions, similarly to any other colloidal particle. The success of the attachment and the potential for detachment is heavily influenced by surface properties such as material type and topography. The growth of the colony is similarly guided by mainstream flow and the convective transport throughout the biofilm. Beyond the growth phase, hydrodynamic traction forces on a biofilm can elicit strongly non-linear viscoelastic responses from the biofilm soft matter. As the colony exhausts the means of survival at a particular location, a set of trigger signals activates mechanisms of bacterial release, a life-cycle phase also facilitated by fluid flow. A review of biofilm-relevant hydrodynamics and startum properties provides insight into future research avenues.

Contents

* Corresponding author.

https://doi.org/10.1016/j.cis.2020.102336

1. Introduction

Bacteria live a fascinating life and have an equally fascinating impact on human life, spending much of their lives as active colloidal dispersions, either in the form of planktonic solutions or as jelly-like biofilms. As planktonic solutions, bacteria can exhibit large scale coherence and even superfluidity [1,2]. In the biofilm form of bacterial aggregation, bacteria live in interface-associated communal colonies. Biofilms are an aggregative form of microbial life, wherein aggregations of microbes are encased in self-secreted extracellular polymer substances (EPS) [3,4]. EPS, which is composed of an assortment of biological macromolecules ranging from DNA to polysaccharides, serves as "biological glue" causing the biofilms to adhere to interfaces and also provides the same with mechanical integrity [5]. Bacterial biofilms, can be thought of as "composites of colloids embedded in a cross-linked polymer gel" [6]; traction forces on biofilms can elicit linear/non-linear viscoelastic response [7]. Bacterial biofilms are ubiquitous in nature and their applications can range from global cycles, waste water treatment, and bioremediation [8], to biomedical [9] and industrial biofouling. In the medical industry biofilms contaminate endotracheal tubes [9], catheters, implants, and cause gum diseases [10,11]. More than 45% of infections in hospitals can be traced back to medical devices, with catheters being the second most dominant source of infection [10,12]. Infected implants often require follow-up surgery, further increasing financial burden and chance of fatality. In the food industry, biofouling can cause taste and odor problems [13], in addition to harboring dangerous pathogens in potable water systems [14]. In the marine industry, micro- and macro-fouling on ships hulls increases drag thereby increasing the operating cost of the vessel. A 15% loss in speed, due to a 80% increase in friction can be attributed to a 1 mm thick biofilm on a ship hull [15]. Additionally, the foulants, if not removed periodically, can deteriorate the host surface, decreasing longevity and compromising integrity.

Biological macromolecules in the EPS are cross-linked by proteins and multivalent cations, and thus the EPS can be viewed as a polymer matrix, whereas the relatively stiffer cells are suspended in this matrix [6]. From the perspective of the microorganism, communal living offers outstanding protective capability. Individual microorganisms that would swiftly perish in an open environment find an excellent support system in the assembly of their own kind. Colonies provide an exceptionally safe environment for their members against external mechanical, chemical, biological, and environmental aggression. A typical biofilm life-cycle, which is shown in Fig. 1, starts with a process in which the cell becomes a part of the colony. Cell movement plays a critical part in the biofilm formative phase [16]. Static cells, whether planktonic or already attached to the surface, have limited means of meeting other cells [17]. Flow in the medium, so called "bulk flow", facilitates cell migration via convection, in addition to cells' own motility exerted through mechanisms such as appendage thrust or surface twitching [16,18–21]. Minutes after scouting a suitable location on an interface for settlement through the process of reversible attachment, a cell will join other cells in irreversible colonization of the surface [22]. As their numbers grow, cells shroud themselves in a protective polymer coating which provides both the chemico-mechanical protection from the environment, and the means to capture a predominately diffusive supply of nutrients [23,24]. Embedded in clusters and covered by the binding substance, bacteria form the biofilm, which allows them to survive far longer than they would be able to do individually [25]. The colony typically matures within several days after which the availability of the nutrients at the current location becomes progressively more limited [26]. When the environmental conditions become unfit for survival, a complex signaling process triggers the release of cells [27,28]. The growth phase

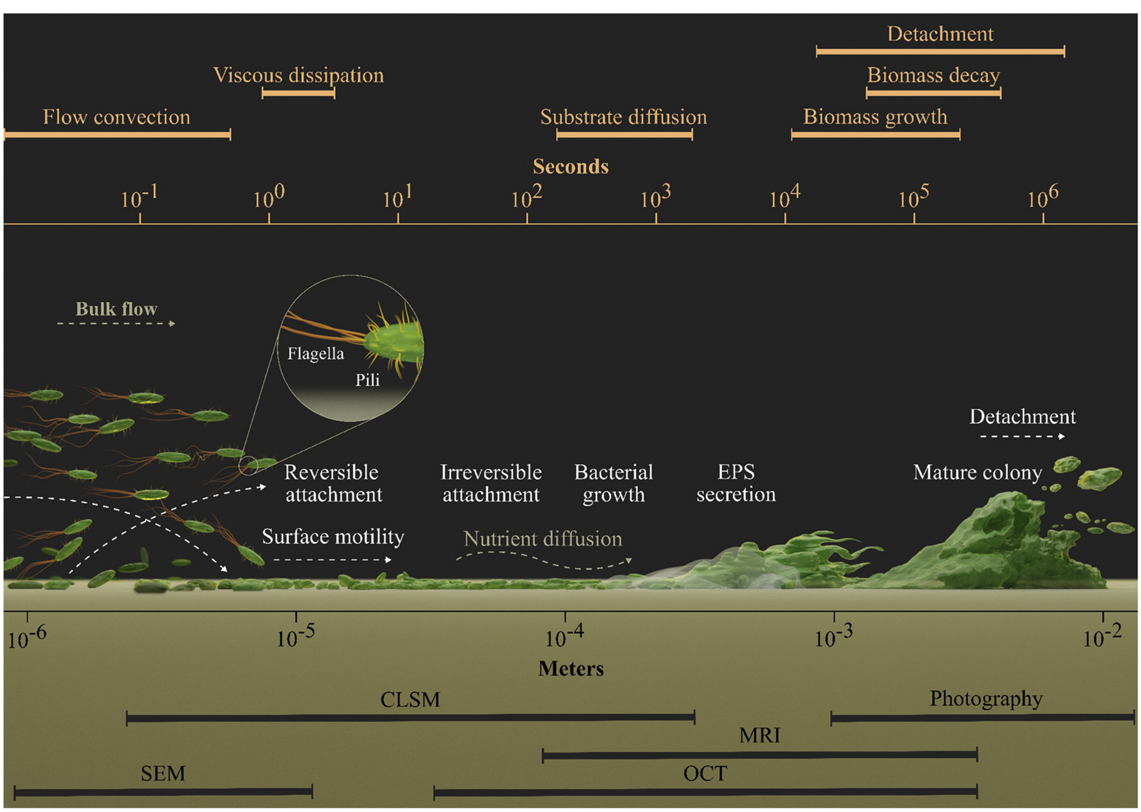

Fig. 1. Relevant physical scales for a bacterial biofilm life-cycle. Phenomena can occur continuously and simultaneously without a clear demarcation on either time- or length-scales, however discrete temporal and spatial intervals can be identified. Mass flow, mass transport, and biofilm growth and disintegration interact throughout the biofilm life-cycle. Visualization method resolution decreases from left to right, and the opposite is true for the field of view. Abbreviations are: SEM - Scanning Electron Microscopy, CLSM - Confocal Laser Scanning Microscopy, OCT - Optical Coherence Tomography, and MRI - Magnetic Resonance Imaging. Adapted from [31–33].

transitions into decay, detachment of dead cells, and migration of living cells to more promising domains. The departure can take the form of a continuous release of cells or an abrupt detachment of a whole cluster [29].

The co-existence of a plethora of concomitant transport and biophysical mechanisms in a biofilm ensures that relevant time- and length-scales span several decades [5,30] (Fig. 1). The time-scale indicates nutrient diffusive transport is much more rapid than biomass growth and release events [31]. In addition, mass transfer by diffusion is significantly slower than the momentum transport mechanisms of convection or dissipation. Also shown in Fig. 1, the biofilm life-cycle spans greatly contrasting length-scales. Individual cells of $O(10^{-6}$ m) create colonies which can span multiple centimeters. Phenomena occurring at one scale typically do not repeat identically at different scales [32]. To properly appreciate the biofilm evolution it is necessary to combine the different visualization techniques across all scales–from scanning electron microscopy for visualizing individual cells through photography to capture the shape of mature colonies.

The ubiquity and persistence of biofilms may not just elicit recognition of certain detriments, but can also carry practical benefits. Engineered uses of organized bacterial activity are found in the form of fuel bioremediation and trickling filtration in waste water treatment [27,34–42]. However, our perspective of structured bacterial behavior is focused on detrimental aspects. The adverse effects of biofouling pervade numerous fields of human activity: health and dental care, marine transportation, water transport and filtration, food production and storage, nuclear and conventional power generation, to name but a few. Consequently, bacterial proliferation is closely accompanied by suppression efforts. Identical external factors can either support or impair the survival of a microorganism, based on a complex combination of circumstances, particular to a specific bacterial species. Among the numerous factors affecting microorganisms in their efforts to establish and retain a congregate shape, and the focus of this review, are two physico-mechanical factors: hydrodynamics and the properties of the fouled stratum. Apart from affecting, often decidedly, all stages of the bacterium life-cycle, hydrodynamics and surface characteristics have the ability to amplify the effects of other chemical, biological, mechanical, or environmental interactions. Previous studies offer comprehensive summaries of various stages of the biofilm life-cycle [11,43–48]. To the best knowledge of the authors, no previous works focus specifically on the combined impact of hydrodynamics and stratum properties. The goal of this work is to concisely review the impact of fluid flow (§2) and surface structure (§3) on all stages of biofilm development: attachment, growth, and detachment.

2. Flow conditions guide every stage of biofilm life-cycle

The abundance of experiments [49–60] performed to study the effect of flow conditions and hydrodynamic forces on biofilm structure consistently arrive at a common conclusion: fluid flow heavily influences biofilm characteristics. Growth rate [33,61–66], structure [33,55,67–70], shape [60,71–73], cell concentration [68,74–76], and detachment [16,22,77,78] are all impacted by bulk flow. Bacteria excretes extracellular polymeric substances (EPS) [19,33,42] to form a protective, heterogeneous structure consisting of both clumped cells and cells dispersed within the EPS matrix. Biofilms with a higher ratio of EPS have greater densities [79]. The matrix comprises up to 80% of biofilm organic matter volume [27] and typically develops into a heterogeneous, corrugated shape traversed by both open, groove-like channels, and tunnels that allow fluid ingress throughout biofilm volume [22,55,80]. The structure of biofilms is discussed in detail in §2.2, and their elemental parts are shown in Fig. 2. Bacterial micro-colonies embedded in cell clusters and condensed sub-layers, are separated from other micro-colonies and planktonic cells in a heterogeneous, mixed-species environment [19]. Open channels and subsurface conduits span the entire biofilm, creating an extensive web of fluid access pathways [4,40,81–85].

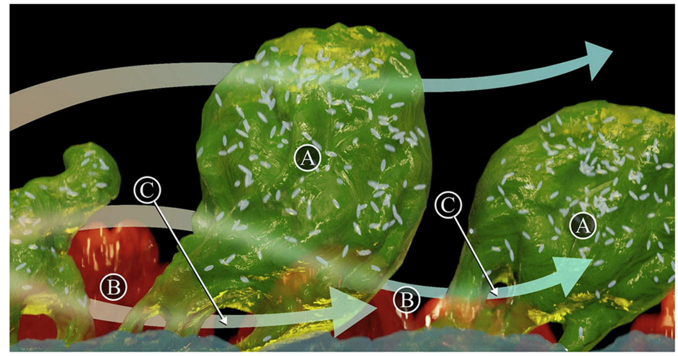

Fig. 2. Basic biofilm structure. (A) micro-colonies grouped into cell clusters. (B) pores and open channels. (C) conduits. Arrows indicate convective flow around and through the clusters. Adapted from [19,86,87].

2.1. Bacterial motility and initial attachment

Fluid motion—as characterized by sedimentation, diffusion, and convection—is the primary mechanism of bacterial and mass transport along a surface [33,88–90], and is schematized in Fig. 1. The dominant transport mechanism for a particular film is partially dependent on the dynamics of the medium - static, laminar, or turbulent [52,53,55,59,91,92]. Flow promotes thicker and denser biofilm growth when compared to static environments [49,50], but this contrast may be time [93], species, and substrate dependent. When compared to static environments, *Candida* biofilms grow to a greater thickness under flow in early growth stages (< 6 h) but are thinner than those in static environments at later stages (24 h) [93]. Flow facilitates bacterial environment sensing and aggregate communication efforts such as chemotaxis and quorum sensing, respectively [21].

Bacterial surface adhesion is complex because it involves different active and passive methods of attachment, such as mass transfer processes, Van der Waals forces, surface hydrophobicity, electrostatic interactions and bacterial deployment of organic adhesives [48]. The ability to attach to a surface stems mostly from bacterium near-surface positioning and motility [5]. Thus, active movement is required for bacteria to draw toward a surface and establish contact, even before the effects of a particular surface material or texture are considered. Following the near-surface positioning activity, the biofilm formation process continues with the initial adhesion of the bacteria to the surface. This activity typically goes through two phases: a reversible and irreversible adhesion [94,95].

The role of fluid dynamics in biofilm formation extends to both motile and non-motile (crippled) cells. Crippled cells, those with immobile or no appendages, rely heavily on the fluid flow to attach to a surface and form a biofilm [16,18–21]. Motile bacteria move autonomously by expending energy and enjoy several survival advantages in static fluids by using their appendages for attachment, detachment, and relocation [16]. In contrast, crippled cells achieve surface contact via cell settling, Brownian motion, and vortex currents, which are most effective at low flow velocities [16]. Non-motile bacteria and diatoms, in absence of convective flow, are particularly susceptible to Brownian motion [75,96–98], the dominant transport mechanism in the initial stages of attachment . Initial attachment is characterized by potential reversibility, where bacteria leave the stratum to attempt recolonization elsewhere, discussed in further detail in §2.3. Reversibility of attachment, as well as the type of near-surface interaction between a surface and the cell, can be anticipated based on microorganism's distance from the stratum [99], which is a result of bacterial motion.

Motile microorganism attachment mechanisms rely on actuating appendages, such as the flagella. Flagella-driven organisms sense (Fig. 3) nearby solid surfaces and can modulate their path toward the surface [100]. Detection of a nearby surface can be achieved via signals from one of three categories: physico-chemical changes, appendage attachment, and body contact [101], as shown in Fig. 3. Near the surface, the fluid micro-environment differs from that of the main body of liquid. Gradients in osmolarity, pH value, ionic strength, and nutrients concentrations are physico-chemical properties that can be sensed by a bacterium, Fig. 3a I. Attachment sensing can be achieved either through appendages such as flagella, pilli (Fig. 3a II), or curli, or through body contact (Fig. 3a III).

Once the hydrodynamic forces deliver a cell near the surface, appendages begin assisting the attachment process. The near field flow and dependence of imposed external forces are affected by cell shape [21], in a process that can be explained with a simple model. Bacterium shape is often approximated as a sphere in conceptual models, as illustrated in Fig. 3b IV, despite cells typically being oblong. During the near-surface movement of a sphere, shear stress increases toward the stratum, where it reaches a maximum. Therefore, the side of the cell closest to the stratum experiences more frictional drag, inciting rotation [100,102]. Non-spherical, or oblong, bacterial cells experience an additional drag-induced torque opposing rotation that is induced by form drag. The equilibrium of skin-friction and form drag torques forces an inclined cell orientation toward the stratum as shown in Fig. 3b V. Further swimming efforts trap cells within a plane parallel to the surface, increasing the residence time and chances of attachment. Depending on the combination of stratum and bacteria strain, their interactions may exhibit existence of what is called the “secondary minimum” in DLVO (Derjaguin, Landau, Verwey, and Overbeek) theory. The secondary minimum is a state of loose, reversible attraction sometimes present at microscopic separation distances. If the secondary minimum is present and if bacterium twitching takes the cell out of equilibrium incline, the cell may further approach the surface and become entrapped by electrostatic and van der Waals forces. In the case where a surface has a significant free-energy barrier, cells will face repulsive forces that keep them captured in the so-called repulsive layer. Where the free-energy barrier is less prominent, cells might approach the surface so close that the primary minimum will trap them in irreversible attachment. Based on these interactions, three layers, or compartments, can be identified: bulk flow, near-surface bulk flow, and a near-surface constrained zone. The boundaries of the layers are defined, in the direction from the main flow to the surface, by: the fluid boundary layer, the secondary minimum, and the free-energy barrier [100]. Beyond 10 μm from the stratum, cells have no interaction with the surface, rather hydrodynamic forces guide movement. Within 10 μm, wall effects on cell movement become increasingly prominent. Still, no other forces act until a 20 nm distance is reached, after which electrostatic forces begin competing with hydrodynamic effects [100]. A similar stratification concept, shown in Fig. 4, has been proposed by another conceptual model which considers a bacterium to be an inert particle [99]. Three separate regions are defined based on the type of interactions between the bacterium and substratum. At distances of >50 nm, the two surfaces are too far apart to engage in short distance interactions between chemically compatible stratum components, or the so called “specific surface interactions”. At this range only the van der Waals forces are relevant. Between 10 nm and 20 nm, electrostatic repulsion becomes relevant, leading to a temporary possibility of reversible adhesion. As cells continue the approach, they encounter a significant and practically impermeable electrostatic potential barrier. The amount of energy required to overcome the barrier becomes prohibitively large at distances of <1.5 nm. Surface structures will instead transform to form small protrusions on the cell surface that will reach substratum through the potential barrier. At this distance, bonding interactions become essentially irreversible [99]. While certain differences can be identified between the two models in terms of the hydrodynamic conditions and the exact separation distances, they both provide insight into the length-scales of the phenomena.

Cells with and without flagella may possess pili. Type-IV pili (TfP) enable motility and attachment, and assists both initial contact and subsequent locomotion across the surface [96]. While the exact process of pili attachment to the surface is not yet precisely described [103], an important tool to achieve adhesion is disulfide-based bonding, executed at an exposed pilus tip [38,104,105], which allows adherence to organic

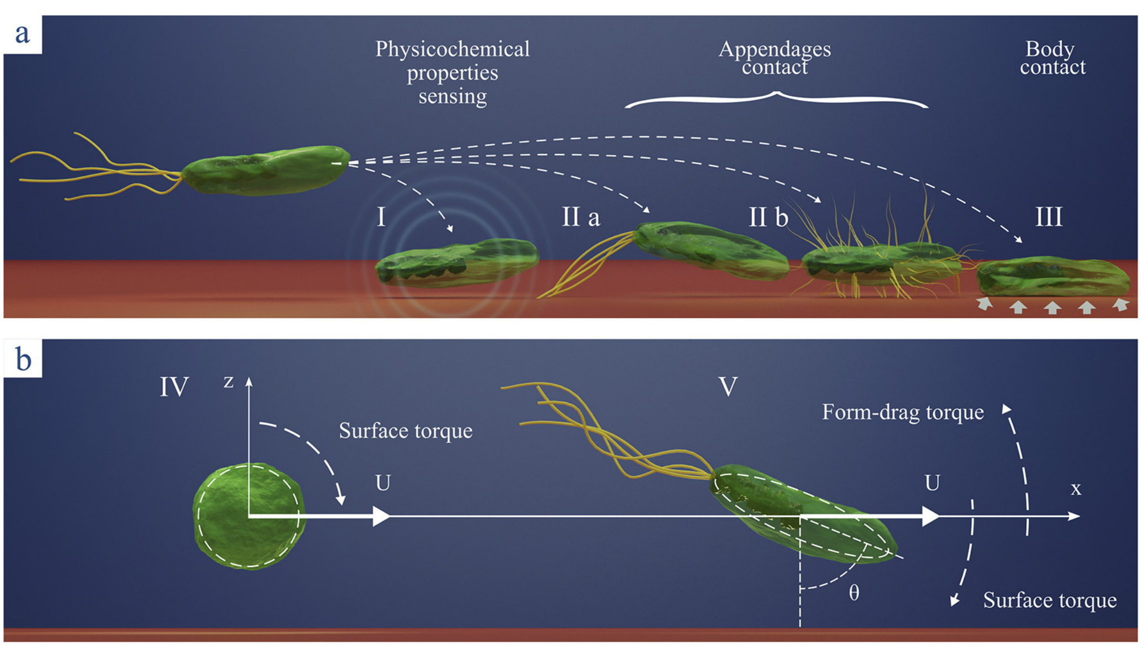

Fig. 3. (a) Cues sensed by a cell approaching the surface. (I) changes in micro-environment, (II) physical contact of appendages, and (III) envelope stress of physical contact. (b) Torques imposed on a cell model moving parallel to a surface at constant velocity *U*. (IV) Surface induced drag torque, causing forward roll of the spherical body. (V) Balance of “surface” and “form-drag” torques acting on a prolate spheroid, directing the body toward the surface at an equilibrium angle (θ). Adapted from [100,102].

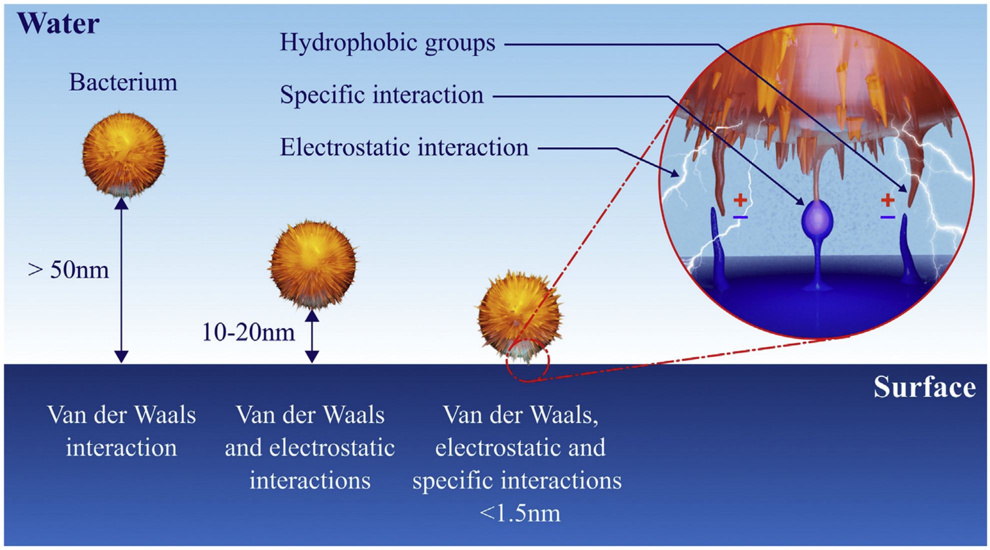

Fig. 4. Regions of interaction between the bacterium and substratum. At separation distances of >50nm (left) adhesion is driven by macroscopic cell surface properties. Between 10 nm and 20 nm (middle) electrostatic repulsion introduces the possibility of reversible adhesion. Under 1.5 nm (right), only adhesion via extruding probes and hydrophobic groups can achieve coupling with the substratum. Adapted from [99].

and inorganic surfaces. Following attachment, cells locomote about the surface by crawling (Fig. 5a) or walking (Fig. 5b), either by retracting attached pili or rooting themselves upward on pili [96,106]. Crawling motion results from TfP retraction which allows cells to drag themselves when lying down (Fig. 5a). This mode of motility, which is enabled by the retraction and elongation of TfP, is known as twitching and can be understood through the coupling of TfP elasticity and interfacial behavior of molecular motors. Models indicate that retraction is reaction controlled and elongation is transport controlled [107]. The number of TfP working together to produce twitching will proportionally affect the linearity and, subsequently, velocity of the movement. Pilus retraction allows *P. aeruginosa* cells to migrate upstream after flow rotates the cell about the attachment pivot point and aligns its forward-facing pole with the flow direction, as shown in Fig. 5c [106]. TfP are also capable of producing a sudden "slingshot" movement. In a TfP bundle under tension, where individual pili branch out in different directions, release of a single pilus results in rapid combined translation-rotation of the cell, as shown in Fig. 5d. In the surroundings of a pseudo-plastic fluid, such as the extracellular polymeric substance (EPS), such swift movement is an efficient transport mechanism [5,108].

Just as hydrodynamics aids attachment, flow can also facilitate detachment. An increase in bulk flow velocity facilitates cells and nutrients transport but also triggers detachment events, as discussed in more detail in §2.3. A balance between the two events is struck at a "critical shear stress" value [109]. In the case of *S. epidermidisHBH276* bacteria growing on silicone rubber, the critical shear stress is 2.7 ± 1.1 Pa but application of polyethylene oxide coating reduces the value to merely 0.2 ± 0.1 Pa [110]. A study conducted with a cylindrical rotating reactor concludes that high wall shear stresses facilitate attachment [110], however another study produced opposite results [111]. While the authors of [111] allowed for the possibility that reduced attachment was a result of increased centrifugal force, others have shown that high shear hydrodynamic conditions can significantly reduce cell attachment [49,112].

2.2. Medium flow and biofilm growth

In the absence of bulk flow biofilms typically take an unstructured [113], isotropic [114] form, given that no other sources of non-homogeneity such as gene expression, genotypic variation [115], mass transfer gradient limitations [116,117] or significant surface heterogeneity are present. Exposed to flow shear, and in concert with a complex array of biological and physico-chemical factors, listed in Table 1, a biofilm will evolve into a complex, heterogeneous shape [23].

Shear stresses associated with laminar flows promote biofilm homogeneity, increased thickness with lower density, reduced nutrient levels, and lower biomass content [51,52,55–57,118]. As biofilm surface shear

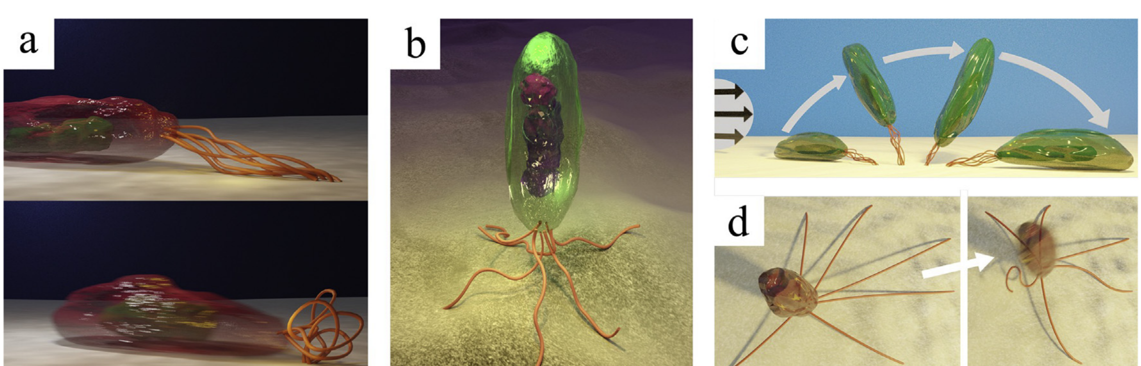

Fig. 5. Pili enabled bacterial movement. (a) dragging. (b) walking. (c) rotation about the point of attachment with the aid of near-field flow. (d) "slingshot" maneuver [96]. Panels (c) and (d) adapted from [106,108].

Table 1
Summary of the factors influencing the formation of biofilms at different times, presented here in its entirety as published in [23].

Genotypic factors	The specific genotype of the organism. Expression of genes encoding surface properties. Expression of signaling systems. Formation of EPS. Organism growth dynamics; specific growth rate, lag periods, afinity for substrates, yield coeffcients etc. Expression of genetic factors not directly connected to biofilm formation (motility and chemotaxis, catabolite repression genes etc.)
Physico-chemical factors	Phase interface (combinations of solid, liquid and gaseous). Substratum composition and roughness. Substrate composition. Substrate concentration/gradient. Temperature, pH, water potential, pressure, oxygen supply and demand, radiation effects.
Stochastic processes	Initial colonization: attachment, detachment. Random changes in biotic and abiotic factors.
Deterministic phenomena	Specific interactions between organisms: competition, neutralism, cooperation and predation.
Mechanical processes	Shear due to laminar or turbulent flow conditions; abrasion; logistic restrictions.
Import-export	Addition or removal of biotic or abiotic components to a biofilm system, E.g. the import of sand, clay minerals or organic detritus into a biofilm structure. Sloughing off of biomass, release of individual (swarmer?) cells.
Temporal changes	Diurnal or annual periodic changes in biotic and abiotic environment, e.g. light, temperature, pH, P_{O_2}. Irregular changes due to unforeseen events.

stresses increase, production of EPS per unit volume rises to strengthen the structure [57]. EPS production increases colony adhesion and cohesion, allowing cells to retain activity within the matrix while increasing their protection from external forces. In contrast to laminar flows, turbulent flows promote denser and slimmer biofilms, with decreased metabolism and fewer cells [53,54,57,58,60,62,78,119–122]. Although increases in shear stress can result in an increased metabolic rate [123,124], it has been demonstrated that greater metabolic activity is unsustainable over longer periods of time [124]. The difference between the structures of biofilms formed in laminar and turbulent flows after seven days of development can be seen in Fig. 6. Turbulent flow across a stainless steel slide shapes a *Pseudomonas fluorescens* colony into a compact structure with higher cell count, Fig. 6a, in contrast to the less coherent structure which forms under laminar flow Fig. 6b.

Biofilm structure is composed of corrugations, pores, and conduits traversing cell clusters [19,23,84–86,126–129]. The influence of high fluid shear on the initial structures formed by colonies of several hundreds of cells is insignificant [130]. Hydrodynamic stresses can cause detachment of portions of the biofilm leading to extended water channels in pre-formed structures [131]. However, hydrodynamic forces affect the development of the bulk biofilm structure in conjunction with factors listed in Table 1. Ingress passages develop even in colonies in contact with air [84]. Ridges and tunnels allow bulk flow to reach intercellular regions toward the fouled substratum, where fluid would otherwise not penetrate [126,132–136]. Facilitation of mass transfer via convective flow through these passages has been proposed [82–84,86,137] because tunnels increase the surface area available to nutrient flux and permit access to otherwise deprived cell clusters [86]. Corrugated structures may also serve as fluid storage [138]. Stagnant medium or low-flow conditions present a barrier to nutrient supply and waste products removal from the colony [90]. The zone of reduced flow above the biofilm surface causes formation of a diffusive boundary layer, lowering oxygen diffusion into the biofilm and establishing steep oxygen gradients at biofilm-medium limits [139–141]. Colonies that absorb nutrients by diffusion have feeding capabilities that scale with surface area and nutrient demand that scales with volume. Therefore shape evolution of the biofilm is critical to avoid starvation [142].

Computational modeling demonstrates that colonies deprived of nutrient flux through external surfaces and internal channels develop more elaborate shapes [22]. In general, transport of nutrients and oxygen by bulk flow is more rapid than transport by diffusion [90] but bulk flow does not penetrate cell clusters, thus rendering convection unable to supply oxygen to the interior of cell clusters [24,90]. Oxygen surface diffusion has its own limitations [143], allowing oxygen to reach only tens of microns into a cell cluster [86] as shown in Fig. 7a. In contrast, direct transport via bulk flow through the outermost biofilm surface is comparable to flux via open channels [86]. In an experiment with biofilms of an unspecified composition, the average oxygen flux in the direction perpendicular to the fouled surface was found to be approximately 2.3× greater than the flux in the parallel direction [86]. A mathematical model investigated the impact of nutrient transport on biofilm growth in a static medium [144]. A decrease in nutrient flux causes the evolution of pillar-like, filamentous protrusions in the biofilm and increase in roughness. Limited exposure to favorable gradients, coupled with gradient orientation toward the surface, guides different parts of a colony to compete for nutrients by growing perpendicular to the fouled surface. The change in shape starves the lower sections of the biofilm due to limited nutrient flux and concentration. Furthermore, the change in structure is followed by a change in orientation of the concentration gradient, as illustrated in Fig. 7b. Concentration contour lines follow the evolving shape, remaining normal to the biofilm surface instead of the fouled surface. The concentration gradient further limits the flux in the lower parts of the colony [144].

The most commonly observed biofilm structural features include simple conical mounds [52,83], pillar-like [29], and mushroom-shaped [19,24,27,40,67,68,83,136,138,146,147] formations that reach a congregate thickness of approximately 100 μm. Irregular shapes leave gaps between features, as illustrated conceptually in Fig. 2 and by a computational model in Fig. 7, which are channels and pores that

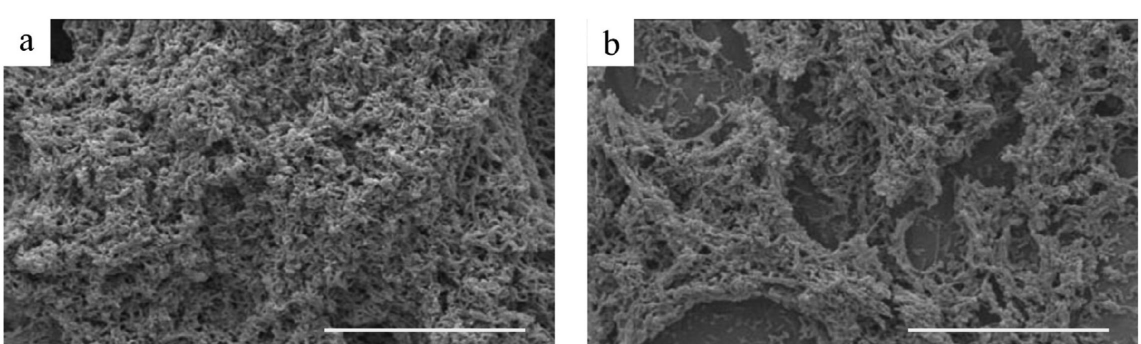

Fig. 6. *P. fluorescens* biofilm formed on stainless steel slides. Shown are colonies cultivated under: (a) turbulent, and (b) laminar flow. Scale bars represent 20 μm [125].

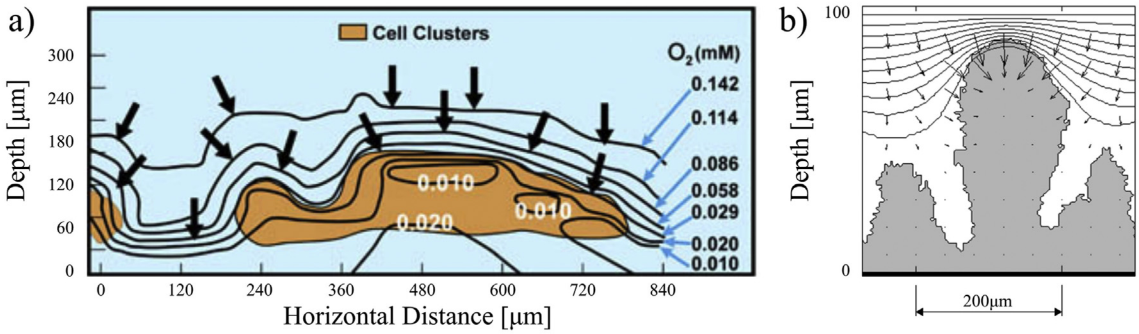

Fig. 7. Nutrient concentration gradients atop the biofilm surface. (a) Oxygen contours and local oxygen concentrations in mM. Arrows represent local gradient vectors. Cell clusters are shown in orange. (b) Two-dimensional model of biomass shape development after 31 days and for group value $G=20$. Lines indicate equal concentration of nutrients, in steps of 10% relative to the bulk concentration. Panel (a) from [145] and based on a figure found in [86]. Panel (b) from [144].

permit fluid access. Laminar and turbulent flow regimes alike may produce wrinkled, ripple-like shapes on the surface of biofilms. Some of the ripple formations formed by *P. aeruginosa* wild-type PAO1 and mutant PAO1-JP1 strains, developed under varying flow conditions in a 3-mm wide by 3-mm high glass flow cell and over different periods are presented in Fig. 8, [68]. Ripples are oriented perpendicularly to the flow direction and migrate with it, which allows biofilm bacteria to advance in bulk along the stratum while avoiding detachment.

The development of biofilm ripples under micro-spray turbulent flows is shown in Fig. 9. High-velocity jet hydrodynamics and their impact on biofilm structure is of practical interest in applications such as dental cleaning [148]. *S. mutans* bioflims exposed to high speed air and water streams develop ripples within milliseconds before fluid causes rupture. Ripple formation is likewise accompanied by biofilm migration downstream. Increase in flow velocity, with Re = 2,667 − 11,935 calculated using a 1 mm gap between two fouled microscope glass slides, progressively changes ripple form throughout the biofilm, including the front of the removal zone (Fig. 9a-g). Similar development is present in *S. epidermidis* biofilms under an identical flow regime, as shown in Fig. 9h. *P. aeruginosa,* however, develops wrinkle-like structures visible in Fig. 9h. Exposed to the jet, a *P. aeruginosa* biofilm does not migrate, nor does it allow for partial material removal but instead detaches in bulk. It is proposed that films are rippled by vortices formed between stratified fluids, the Kelvin-Helmholtz instability [149,150].

Traction forces exerted by fluid flow near a biofilm can often cause development of filamentous, thread-like structures called streamers [151–157]. Streamers are distinguished from biofilms simply by their conspicuous morphology - a result of fluid-active matter interaction. The strong coupling of hydrodynamic traction forces with non-linear material response to stress makes streamers an interesting and challenging topic of research. Bacterial streamers have been reported to form in a very wide range of Reynolds numbers (Re), from creeping flows in closed channels (Re << 1) [131,157–160] to turbulent flows in natural and laboratory conditions [161–163]. Their streamlined structure promotes rapid proliferation of bacteria in closed channels [131,158,164], and the failure of streamers can lead to the advection of biomass, clogging conduits [164,165] and micro-separation devices [159,160,166–168]. In all flow regimes, sustained traction forces, generated by the hydrodynamic flow elicits a time-dependent response from the viscoelastic biomass [6,7,169]. One model that describes the viscoelastic character of a wider assortment of biofilm structures is based on the assumption that biofilms can be viewed as associated polymer networks that exhibit adhesive and cohesive strengths under fluid shear stresses [170]. Upon exposing the colonies to wall shear stresses in the range of 0.005-5.3 N/m it was concluded that biofilms behave as viscoelastic fluids, demonstrating both unidirectional flow as well as elastic and viscoelastic recoil. The material complexity of the biofilm matter is often reflected in both elastic and viscous response of the biomass. Barai et al. (2016) [7] have investigated strain stiffening behavior of biofilms under applied shear loads, which likely occurs due to the unfolding of the biological macromolecules in the EPS. Others have have shown the hyperleastic response of bacterial flocs [158] can result in streamers, which once formed can exhibit complex creep response [165]. Despite some progress, understanding how the interplay of hydrodynamic interaction with a living complex fluid leads to streamer formation remains an challenging domain.

Streamer length can span several orders of magnitude: from microns [71,167,171,172] and millimeters [20,162,168,173] in bacterial films, to several centimeters [56,151,152,174] in algal films. Colonies exposed to turbulent flow conditions evolve filamentous shapes under the influence of high shear stress [73,162,163]. Streamers will start to oscillate

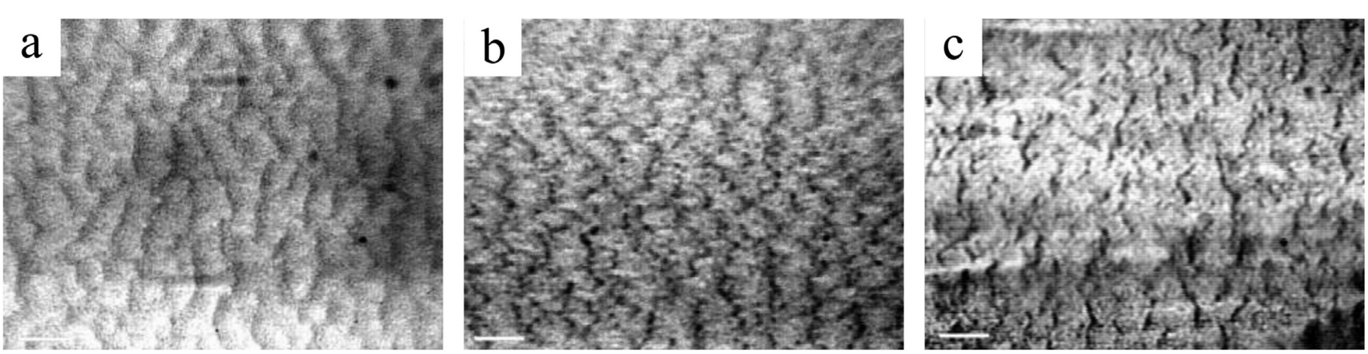

Fig. 8. Ripple structures formed by *P. aeruginosa.* (a) PAO1, laminar flow, Re=100. 5 days, (b) PAO1, turbulent flow, Re=3000, 4 days. (c) JP1, turbulent flow, Re=3000, 6 days. Flow direction is from right to left. Scale bars represent 200 μm. Images from [68].

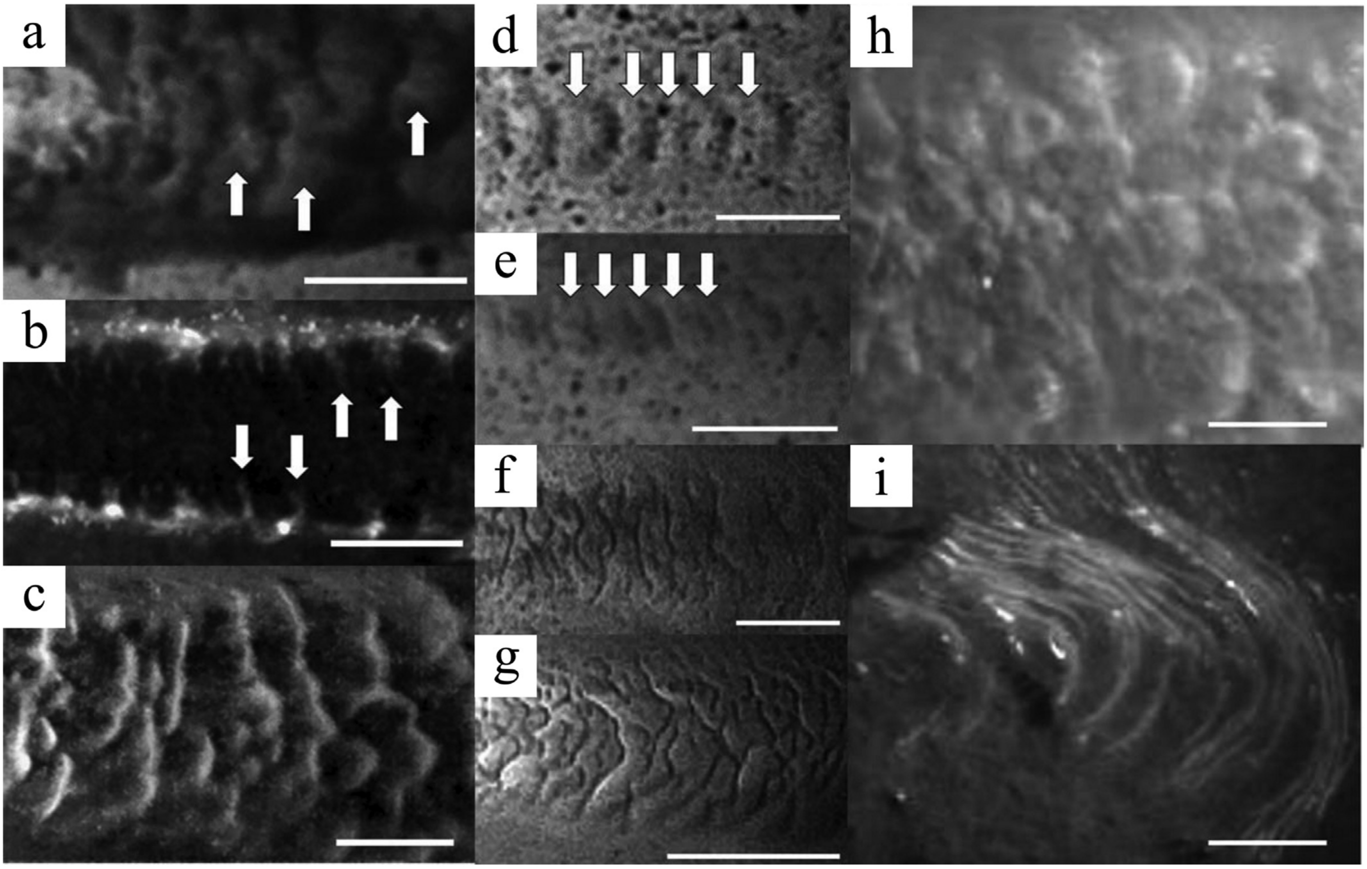

Fig. 9. Ripple-like biofilm formations developed under micro-spray flows. (a-c) *S. mutans* biofilms. Flow direction is from left to right. Scale bars represent 2 mm. (a) Crescent-shaped ripples developed under water micro-spray. Arrows indicate the front edge of the burst. (b) Arched ripples developed under air micro-spray. Arrows indicate ripples at the edge of the clearance zone. (c) Crescent-shaped ripples developed under air micro-spray. (d-g) Progress of *S. mutans* biofilm ripple growth with increase in air stream velocity. Scale bars represent 5 mm. (d,e) Parallel ripples developed under low-velocity streams at 24.6 m/s and 44.9 m/s, respectively. Arrows indicate the front edge of the air micro-spray. (f) Conversion from parallel to crescent-shaped ripples at 85.5 m/s. (g) Crescent-shaped ripples developed in high-velocity stream at 110.1 m/s. (h,i) *S. epidermidis* biofilm ripples and *P. aeruginosa* biofilm wrinkles, respectively, developed under air jet at 85.5 m/s. Figure from [148].

and shed vortices once their length and local flow velocity reaches a critical point [175]. Oscillatory movement introduces pressure fluctuations [73] and enhances mass transfer with the surroundings, including the exchange of nutrients [138]. The convergence of microfluidics and biofilms research [5,30] opened new vistas for investigating the effect of geometry and laminar flow conditions on proliferation of biofilm colonies. At the microscale, streamers were found to form readily in complex geometries such as in curved microchannels [71,176], in porous media mimics [131,157,158] and microfiltration mimics [160,167], and occasionally in straight microchannels [64]. Some examples of such streamers are pictured in Fig. 10. Streamers formed by fluorescent *Pseudomonas flourescens* in a porous media mimic containing PDMS micropillars imaged using confocal laser scanning microscopy are shown in Fig. 10a. While biofilm formation on channel and micropillar walls can be clearly discerned, thread-like streamers, whose ends were tethered to the micropillar walls were observed after several hours of experiment initiation. These streamers rapidly proliferate and grow to clog microfluidic devices much faster than biofilms growing under quiescent conditions [131,158]. Similar streamers in curved microchannels are shown in Fig. 10b,c. The biomechanics of streamer inception remains a contemporary challenge, although a floc-driven streamer formation mode has been clearly identified. Hassapourfard et al. (2015) [158] showed that bacterial flocs introduced to creeping flows in a microchannel can attach to channel walls and then be 'extruded' by hydrodynamic traction forces to form streamers. Here, the ability of flocs to sustain very large deformations played a crucial role in streamer formation. Biswas et al. (2016) [165] later showed that such streamers can undergo complex creep response resulting in fracture and debris transport downstream.

The streamers described above are byproducts of biophsyical phenomena, but Debnath et al. (2017) [177] have recently demonstrated that similar morphological structures can form in particle-laden polymeric flows. Specifically, they showed that when 200 nm amine-coated polystyrene particles (PS) were introduced in a microchannel along with a aqeuous solution of high molecular weight (weight-averaged molecular weight ~ 23 million g·mol^{-1}) polyacrylamide (PAM) solution, the particles aggregated to form a filamentous structure reminiscent of bacterial streamers. The generalization of bacterial streamers beyond the biological domain and into the realms of the more general class of soft materials represents an important development in this field. Kumar and Ghosh, co-authors of this manuscript, have suggested 'colloidal streamers' to supplant the more restrictive bacterial streamers terminology. Abiotic 'colloidal streamers' have implications for clogging of membranes [159,178].

Advantages of increased biofilm surface area should not be indiscriminately assumed. An increase in biofilm roughness alone does not always result in increased nutrient transfer [180]. In a heterogeneous biofilm landscape, overall transport rates are affected by factors such as bulk and pore flow velocities, roughness, and biofilm density. While rougher biofilms increase medium contact area, a part of direct transfer via bulk flow is lost to less effective convective transport in crevices. A diffusive boundary layer may be unable to closely follow a complex biofilm contour, especially at higher velocities. When a diffusive boundary layer remains parallel to the fouled surface the exchange area is

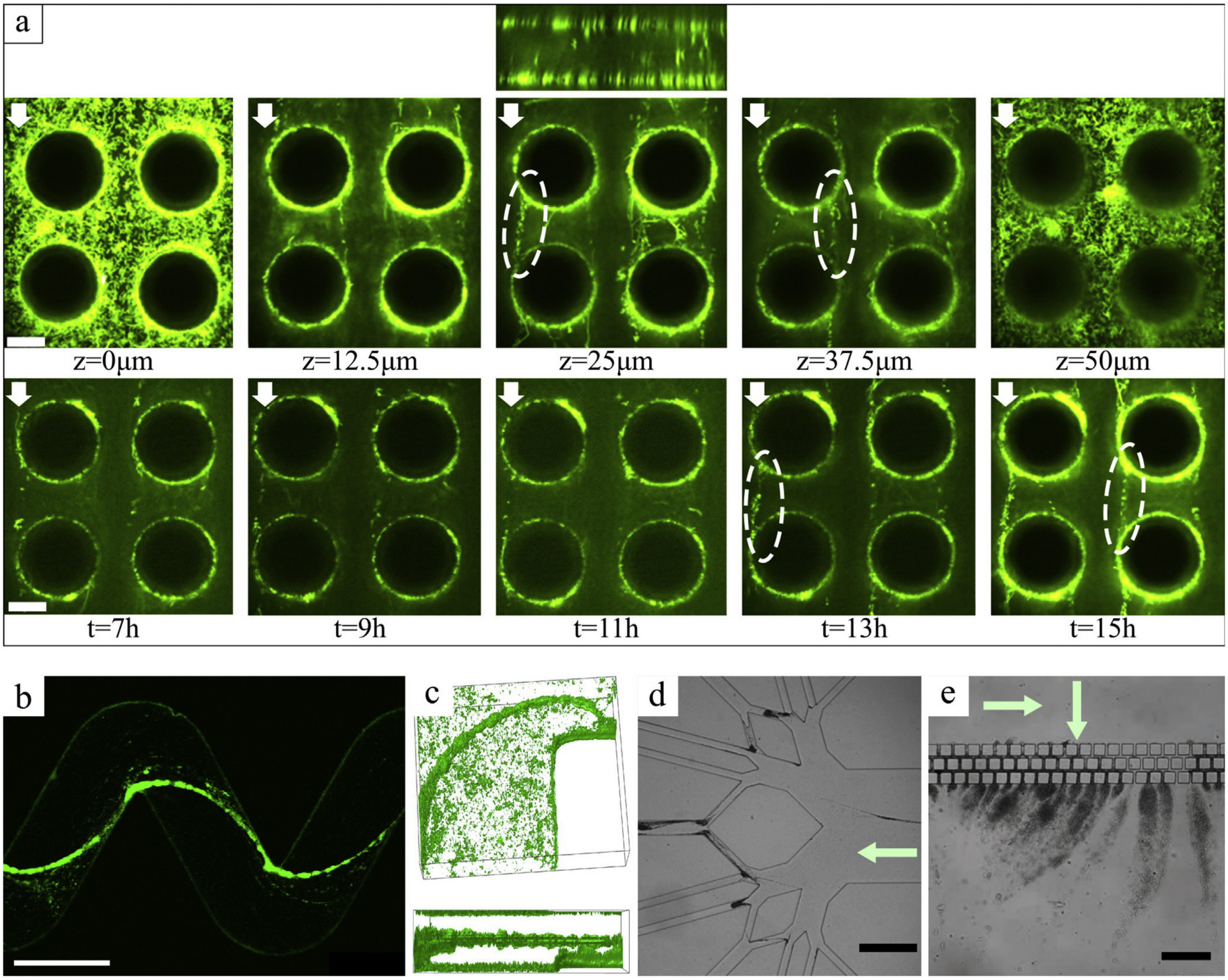

Fig. 10. Laminar flow streamers. (a) Streamer formation in a porous microfluidic device. First row: confocal images of streamers at five different z-locations of the channel, Z = 0, Z = 12.5, Z = 25, Z = 37.5, Z = 50 μm after 15 h of experiment. Confocal sidebar view shown on top. Second row: time evolution of streamers at the flow rate of 8 ml h^{-1}. White arrows show the direction of the flow, and the scale bar represents 20 μm. Dashed outlines highlight some of the streamers. Adapted from [157,179]. (b) Confocal microscopy image of streamers formed in a zig-zag channel, scale bar represents 250 μm. (c) Three-dimensional view of channel and of its cross-section with streamer forming at bend. (d) Streamer fouling of a branched network with green arrow indicating flow direction, scale bar represents 500 μm. (e) Streamer fouling of a staggered-channel filtration device where green arrows indicate pseudo-cross-flow direction, scale bar represents 500 μm [167]. Panels (b), (c), and (d) previously unpublished.

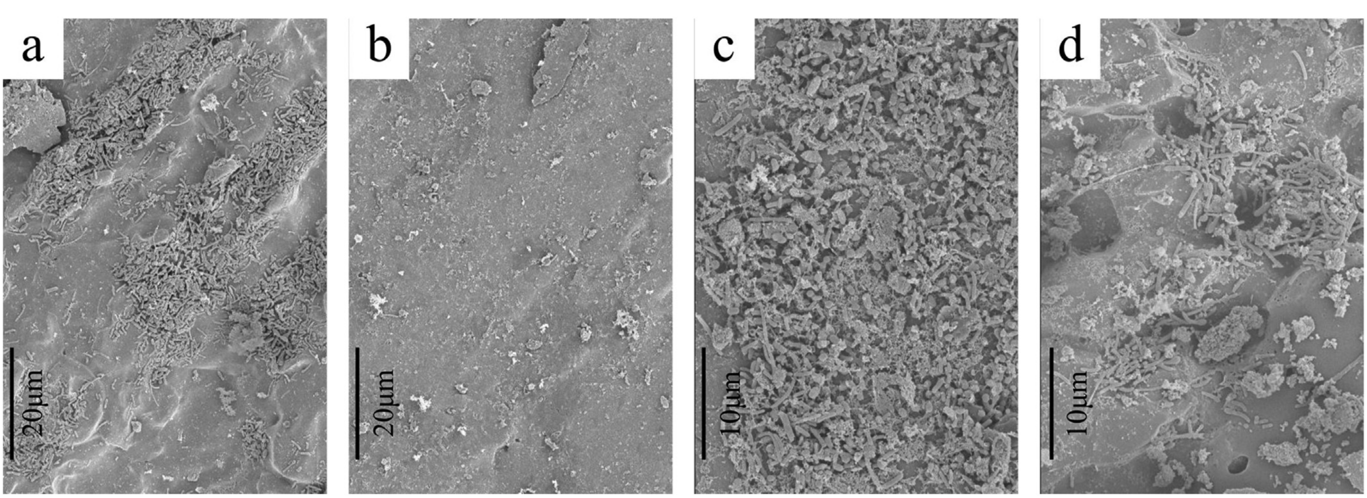

Fig. 11. *L. innocua* biofilms developed under turbulent flows. (a) Re = 9500, 1 day. (b) Re = 16,500, 1 day. (c) Re = 9500, 7 days. (d) Re = 16,500, 7 days. Figure adapted from [187].

effectively reduced, as only the peaks of the biofilm structure reach favorable concentration gradients. Similarly, densely-arranged structures create confined valleys and basins that are separated from the diffusive boundary layer and have limited access to nutrients [180].

An increase in bulk flow velocity promotes mass transfer, regardless of Re [74,163,181,182]. While more biomass is produced at lower flow rates [53,77,183,184] where shear stress rates are lower [61], the proliferation rate increases with bulk flow velocity [53,185]. Growth rate acceleration is a result of an increase in biofilm density [53], due to higher population and greater division rates per unit area. Structures formed under faster flows are thinner [186] and absorb nutrients more readily, accelerating growth rate. However, high nutrient concentrations, while promoting growth, also produce colonies with lower adhesive strength [156].

Some examples of biofilms formed in turbulent flows are shown in Fig. 11. In tests with L. *innocua* cells and stainless steel coupons located in 0.1-m inner diameter tubes, lower Re flows led to more fouling, as seen on Fig. 11a,b [187]. While substantial parts of the coupon fouled at Re = 9500 (Fig. 11a), biofilm formations at Re = 16,500 (Fig. 11b) are limited to several scattered colonies. Over the next six days both biofilms evolved in size, but retained the initial configurations: lower Re flow allowed biofilm to spread evenly across the plate (Fig. 11c), but the colony subjected to high Re developed patchy and more heterogeneous (Fig. 11d). In both cases, colonies took their near-final shapes after four days, and retained those shapes with little to no change henceforth [187].

Fouled surface frictional resistance depends on flow velocity and the biofilm thickness [188]. Thicker biofilms typically produce greater effective roughness, or drag [189], and as mentioned above are formed at lower shear [190]. The effective roughness height of a fouled surface can be more than five times greater than the thickness of the foulant, which can result in a threefold increase in frictional drag when compared to a smooth wall [191]. Thus, biofilm skin friction factor is dependent not only on roughness, but also thickness [192]. Investigation of turbulent boundary layers formed above a biofilmsurface reveals an increase in the skin friction coefficient from 33% to 187% in flows with Re = 5,600 − 19,000, measured at three downstream locations on the flat plate: 1.13 m, 1.43 m, and 1.73 m [192]. Turbulent flow over surfaces protected with adhesion-reducing coatings, or FR coatings, produced skin-friction that was up to 65% greater than the clean surface [193]. The experiment revealed that the friction increased together with the channel-height Re and the combined factor of mean foulant thickness and the percentage of foulant coverage. In a similar investigation, filamentous biofilms produced the drag that was up to three times that of a smooth surface [194]. In contrast, when the drag was measured across a manufactured, rigid replica of the biofilm structure, drag decreased by approximately 50%. The difference in drag values is attributed to the absence of compliant behavior of the true biofilm. The Darcy-Weisbach friction factor changes with Re [188], increasing with Re until a particular threshold value is reached, at which time shear stresses initiate biofilm detachment [156,188]. The detachment tipping point has also been reported for other type of environments, such as micro-filtering devices [156] and other types of microorganisms, like diatoms [184]. Friction factor will begin to decrease past the detachment point, as biofilm starts to break apart [188]. Therefore, the Colebrook-White equation is not applicable to be used in the case of biofouled pipes, and caution should be exercised in practical applications [188]. A combination of factors listed in Table 1 often has synergistic impact on the process of biofilm attachment and growth, due to process complexity. As evident from an experiment performed with *Ulva* zoospores and *Cobetia marina* cells, the attachment rate scales inversely with substratum roughness, and is inversely proportional to the product of engineered roughness index (ERI) and bacterium Re [195]. Orders of magnitude of Re, calculated for a case of uniform flow across the flat plate, were 10^{-3} and 10^{-4} for *C. marina* and *Ulva* cells, and characteristic lengths of $L = 2\,\mu$m, and $L = 5\,\mu$m, respectively, while surface engineered patterns were comparable in scale to the ones discussed in §3.2. Similarly, an inverse linear relationship exists between the biofilm accumulation rate and the bulk flow Re [196].

Most of the experimental insight on the impact of flow regimes on biofilm growth in controlled, laboratory conditions comes from two types of flow systems: linear flow cells and rotating annular reactors. Annular reactors also provide insight into how the complexity of biofilm structure escalates with an increasing complexity of flow conditions. Seemingly simple flow such as the one generated between a static and a rotating cylinder of a reactor creates biofilm structures reported to be as heterogeneous with patches and isolated groups of bacteria, linear marks and structures, streamer-like appendages, and circular and cross-wise shapes; all in addition to an overall height gradient between the leading edge and the downstream end of a coupon [197–199]. When these laboratory testing conditions were made more intricate in an effort to simulate in-situ conditions by adding colloidal particles, such as soil or minerals to the media, biofilm structures became yet more complex [198].

2.3. Shear stress, chemical signaling and detachment

Under varying flow conditions, the initial homogeneous growth phase of a biofilm is followed by a heterogeneous "quasi-steady-state" phase characterized by spontaneous detachment events. If shear forces continue increasing, the biofilm will ultimately reach the so-called "washout" phase, with removal of larger blocks of biomass [200]. These three phases loosely correspond to three stages in the biofilm life-cycle: initial adhesion and growth, peak growth and propagation, and maturation with detachment [201]. The exact mechanisms driving the egress of cells from a colony are not well-understood [99], and while fluid shear alone does not have the ability to cause a catastrophic erosion [79] it is known that hydrodynamics strongly influence the detachment process [200]. Detachment may occur as a result of applied mechanical forces or as a reaction to changes in the surroundings. Cell escape is therefore a deliberate action guided by signaling, cue sensing, and physiological changes. As such, the detachment process is not comparable to attachment in reverse [29]. Different cell escape mechanisms are illustrated in Fig. 12. Removal of biomass may be either by continuous dispersion, or discrete detachment whereby parts of a colony are removed by abrasion, grazing, erosion or sloughing [29]. The fundamental difference between dispersion and detachment is that dispersion is an active process. Microorganisms sense signals from the changing environment [202] which prompts physiological transformations required for cell release. The active process of cue sensing and escape separates dispersion from the desorption, another passive process of escape. Desorption occurs during the reversible attachment phase, as shown in Fig. 12, and is guided by external factors. Dispersion, on the other hand, is a result of cel transformation, does not require the cell to be motile to escape, and thus may be seen as a basic reversal of the attachment process [29]. Dispersion and disintegration work in concert but can produce counter-intuitive events. For example, a sheltered biofilm section, exposed to lower flow rate and therefore lower shear stresses, may fail and detach before sections that are exposed to greater blunt forces. Lower availability of nutrients, limited growth opportunity or perceived risk of starvation will trigger the migration event, even if there is no coercion by mechanical force [203]. When mechanical force is applied, it significantly increases the amount of detached biomass [204–206]. In addition, a combination of high shear and other removal methods drastically improves expulsion of attached matter, as demonstrated in experiments with sonication [206] or disinfectants such as peroxygen [207].

Detachment events are heavily influenced by biofilm growth history in the context of flow conditions, due to the presence of so-called "primary" and "secondary" structures in biofilms [209]. The two types of structures, which are shown in Fig. 13, differ in terms of: growth history, whether they allow the flow to reestablish the upstream profile after

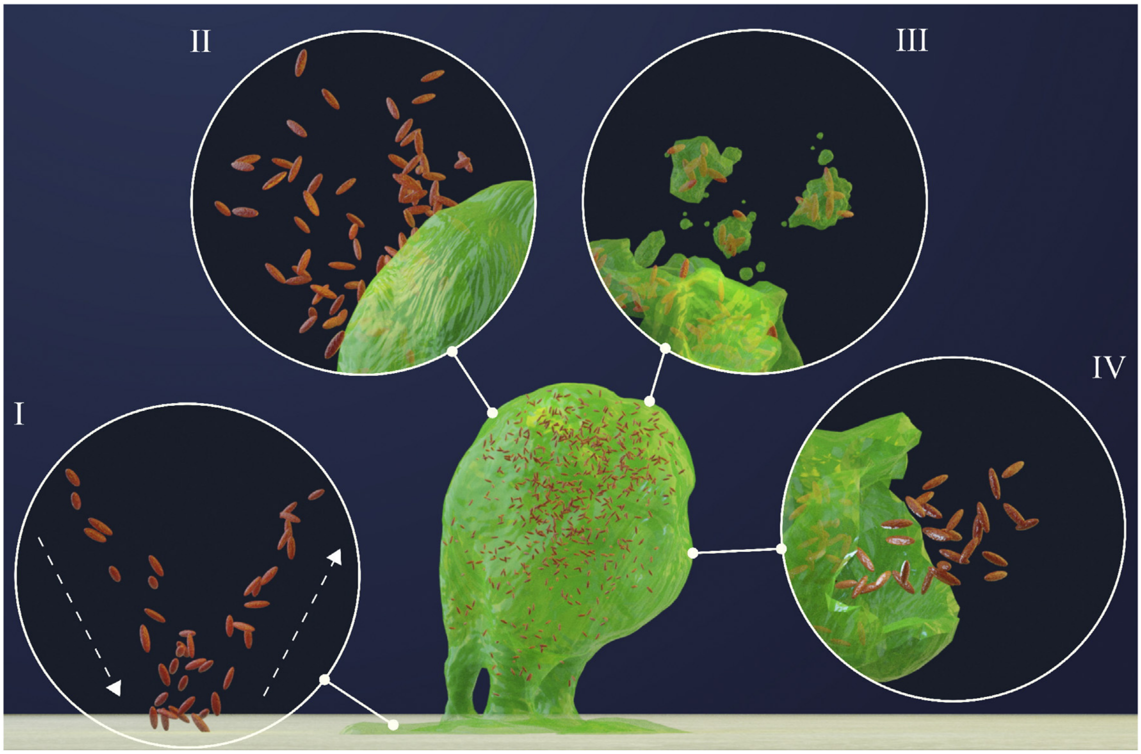

Fig. 12. Methods of cell eviction and evacuation. Before biofilm maturation, cells may leave the surface in a passive process of desorption (I). Once biofilms mature, cells may leave the colony either forcefully by abrasion, grazing, erosion (II) or sloughing (III) detachment, or intentionally through dispersion (IV) in response to environmental changes. Adapted from [29,146,208].

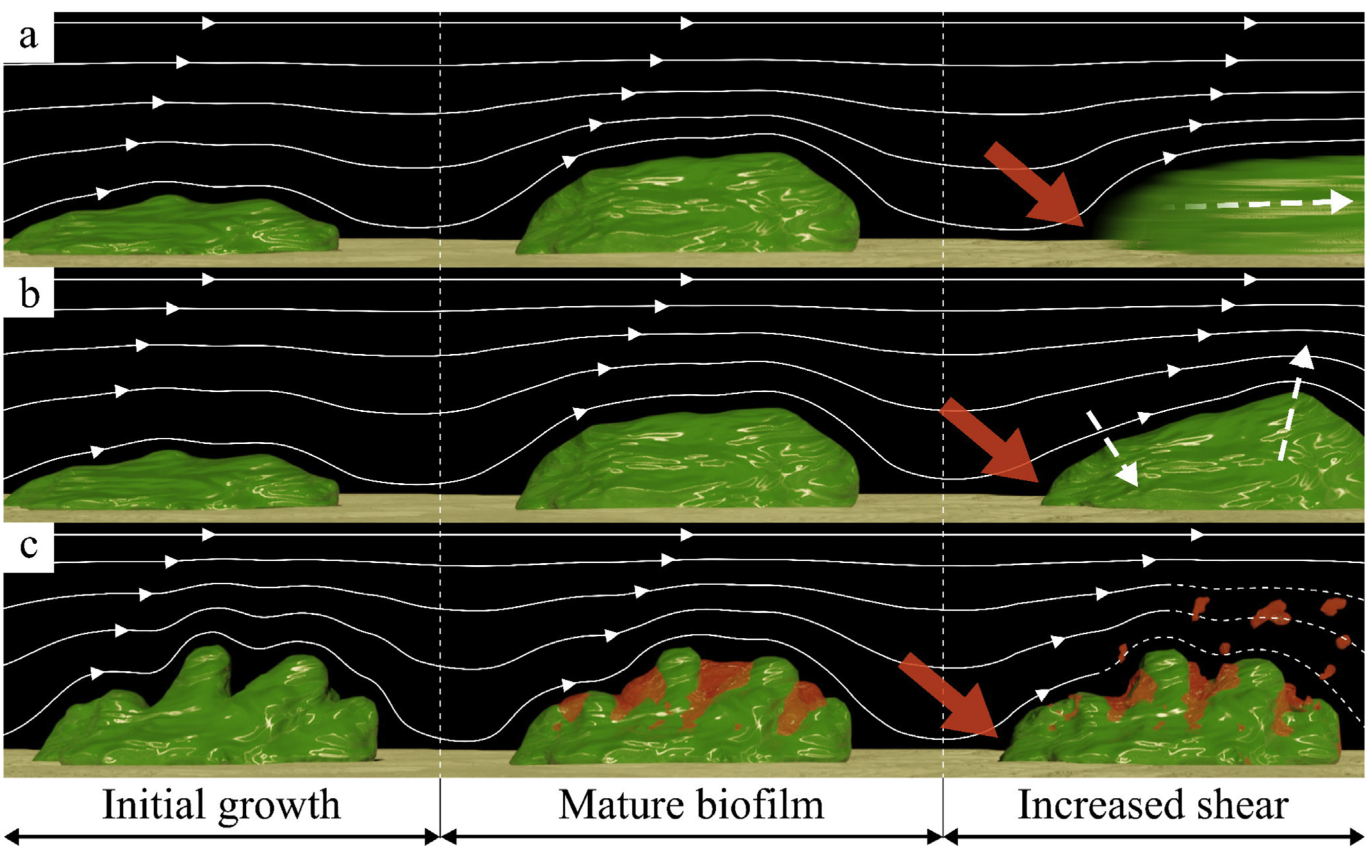

Fig. 13. Primary and secondary structures, shown in green and orange color, respectively. Primary structures include transport voids and channels, and secondary structures amplify local shear forces. Arrows indicate points of higher localized shear stress. Shear stress causes: (a) bulk displacement, (b) in-place deformation, or (c) partial disintegration of the secondary structures. Adapted from [209], and based on data from [210].

encountering the structure, and how they affect the hydraulic stresses at points where fluid first meets the structure. Biofilms exposed to backwash flow during the initial growth phase (Fig. 13c) develop a more heterogeneous surface topography compared to biofilms that form under unidirectional, uniform flow (Fig. 13a,b). Reaching maturation, both types of biofilms grow to a similar thickness – homogeneous biofilms by way of regular growth (Fig. 13a,b), and heterogeneous biofilms by way of the formation of the secondary, filler structures (Fig. 13c). Secondary structures streamline the flow around the biofilm, allowing the flow to reestablish more rapidly compared to flow across a bare primary structure. The recovery of the flow profile results in local shear stresses that exceed those acting on clean surfaces. Bare primary structures will, in contrast, create continuous disturbances to flow but at lower stresses. Application of increased shear stress causes the homogeneous structure to either detach in bulk (Fig. 13a) or remain in place, resisting dislodgement (Fig. 13b), conserving overall volume in both cases. Under the same force, secondary structures will fail and detach first (Fig. 13c). Therefore, biofilms that have been exposed to periodic counter-flow or backwash will develop significant susceptibility to sloughing and detachment of regrown portions of the structure [209].

Under unidirectional bulk flows, high shear conditions can significantly alter both the accumulation and removal rate of the microorganisms depending on the fouled surface roughness and the type of strain of the fouling bacteria [211]. *Pseudomonas genus* is abundant in water supply systems due its ability to generate large quantities of EPS. In absence of protection in the form of surface topography, the ability to generate EPS will diminish when wall shear stress threshold exceeds 0.24 N/m^2 [183]. The choice of substratum material results in growth intensity variance under similar flow conditions, even for identical bacterial cultures [183].

Bacteria concentration in the bulk fluid increases with shear stress, however cell concentration in the biofilm decreases [53]. In an experiment with bulk water heterotrophic plate count (HPC) bacteria, specific growth and release rates remained constant when fluid velocity doubled. However, another identical velocity increase caused both growth and release rates to double [53]. Specific release rate, or detachment rate, is therefore dependent on the specific growth rate [53,58]. Consequently, greater shear stress thins biofilms and dictates their streamlined shape. Colonies retain their structural integrity at relatively high flow rates but are susceptible to relocation under the resulting shear stress [212]. In another experiment, a colony of *Pseudomonas fluorescens* was exposed to bulk flow velocity of 2.8 mm/s in a 2×0.3 mm conduit, and shear stress of less than 53.5 mPa. The colony moved approximately 20 μm downstream while maintaining the overall shape. Upon reducing the velocity and shear to a minimum of 0.28 mm/s and 5.35 mPa, respectively, the bacteria nearly returned to its original position [212]. Biofilm mass shifts become irreversible at a certain flow rate and significant deformation of the structure occurs. Locally tall biofilm colonies partially detach and dangle downstream, in a process that becomes more prominent the taller the biofilm structure. Such abrupt detachment of biofilm fragments represents another mechanism of streamer formation under flow, in addition to continuous elongation discussed in §2.2 [64,212].

3. Biofilm success is conditioned by substrate characteristics

Biofilms form on surfaces with a vast range of physical and chemical properties [213–215]. In the lab, biofilms are routinely cultivated on glass and plastic surfaces of flow cells, coupons, reactors or slips [50,132]. In marine environments, bacterial or diatom biofilms are observed on submerged metal surfaces, both with and without anti-fouling coatings, as well as on wood, polystyrene, and granite [216]. Concrete fresh water transportation networks also suffer from biofouling [217], and similar to marine environments, various anti-fouling coatings also succumb to biofilms, given sufficient time [189]. Closed conduit water distribution systems suffer the same fate across a spectrum of materials including polyvinyl chloride (PVC), cross-linked polyethylene, high density polyethylene (HDPE), polypropylene (PP) [183,218–221], glass [222], cement, iron [201], galvanized [223], and stainless steel [224]. Natural latex has been removed from use in plumbing networks due to the susceptibility to fouling [225]. Soil bacteria will form biofilms on silica and other sand substrates [226], and it is also possible to grow *P. aeruginosa* biofilms on polytetrafluoroethylene [227]. Biofilms on implantable devices pose infection risk to hosts, growing on materials including polyetheretherketone (PEEK), blasted PEEK, commercially pure titanium, and titanium alloys [228], as pictured in Fig. 14.

Given the assortment of materials susceptible to biofouling, it is perhaps more succinct to itemize those which hinder biofilm growth. Investigation of marine biofilms shows that while cell counts in biofilms that form on polyethylene terephthalate (PET) plastic can be higher compared to those that grow on metallic and wooden substrates, their biomass is actually lower. The contrast in film characteristics on plastics versus metals and wood further extends to macrofouling, as plastic surfaces are more resilient to colonies of multi-cellular species such as barnacles. Plastics such as PET and polyethylene (PE) are more susceptible to bacterial biofouling but contain 50% the fouling biomass of steel and 63% of that formed on wood, that are more conducive to the attachment of macrofoulers [229]. Physical instability and degradation of plastic materials appear to decrease their resistance to biofouling, while biofouling enhances the degradation process [230,231]. An interesting comparison between plastics and steel can be drawn in plumbing systems where ratios of biofilm to planktonic microflora vary depending on the particular type of the plastic or steel exposed to microorganisms [225]. Despite the above notes on latex, rubber has been found to be resistant to biofilm formation, at least to *S. paucimobilis* [220]. Copper, copper alloys, and brass stand out as materials that significantly resist fouling by certain bacterial strains, such as *Legionella pneumonia* [232–234]. This characteristic of copper is hypothesized to come from the bactericidal properties of copper [234,235]. Aluminum containing silicates and oxides exhibit total resistance to fouling in-situ, and the attraction to microbial colonizers rises with the increase in iron within applied coatings, attributed to the nutritious characteristic of iron rather than biocidal property of aluminum coatings [236].

Smooth surfaces, where topography has been excluded as a factor in bacterial colonization, will repel or attract fouling cells based on surface wettability. *E. coli*, a hydrophilic electron-donor, will form clumps on surfaces coated with a hydrophobic chemical, such as C3, and branch into threadlike shapes on hydrophilic surfaces coated by NH_2. At the same time, these morphologies share similarities with thin polymer films formed during dewetting of the same surfaces [146].

3.1. Surface energy and initial attachment

Surface energy is a critical factor in the ability of microorganisms to attach to substrates [237]. The majority of studies agree that the conduciveness of a substrate to bacterial adhesion reduces with low surface free energy [238–244]. However, a few studies show conflicting results [245,246]. A clear relationship between surface energy and bacterial adhesion, specifically for *E.coli* and *P. aeruginosa*, is catalogued in Zhang et al. (2013) [247], who confirmed a previous study [248] that a surface free energy between 23 and 30 mN/m produced the lowest bacterial adhesion. The lowest *E. coli* adhesion is reported for surface free energyof 21-29 mN/m [249] while for *Pseudomonas aeruginosa* it is 20-27 mN/m [250]. The study of surface energy/adhesion relations is motivated by the practical design of surfaces that allow vibration and shear to easily clean surfaces with low interfacial attraction. For instance, a membrane with low surface energy was developed for ultra-filtration applications and will not foul [251]. For minimum fouling of bacteria, an optimal surface free energy ranges 20-30 mN/m [247–250,252–254].

Surfaces with low free energy are known to be hydrophobic [255]; water contact angle is inversely proportional to the surface energy

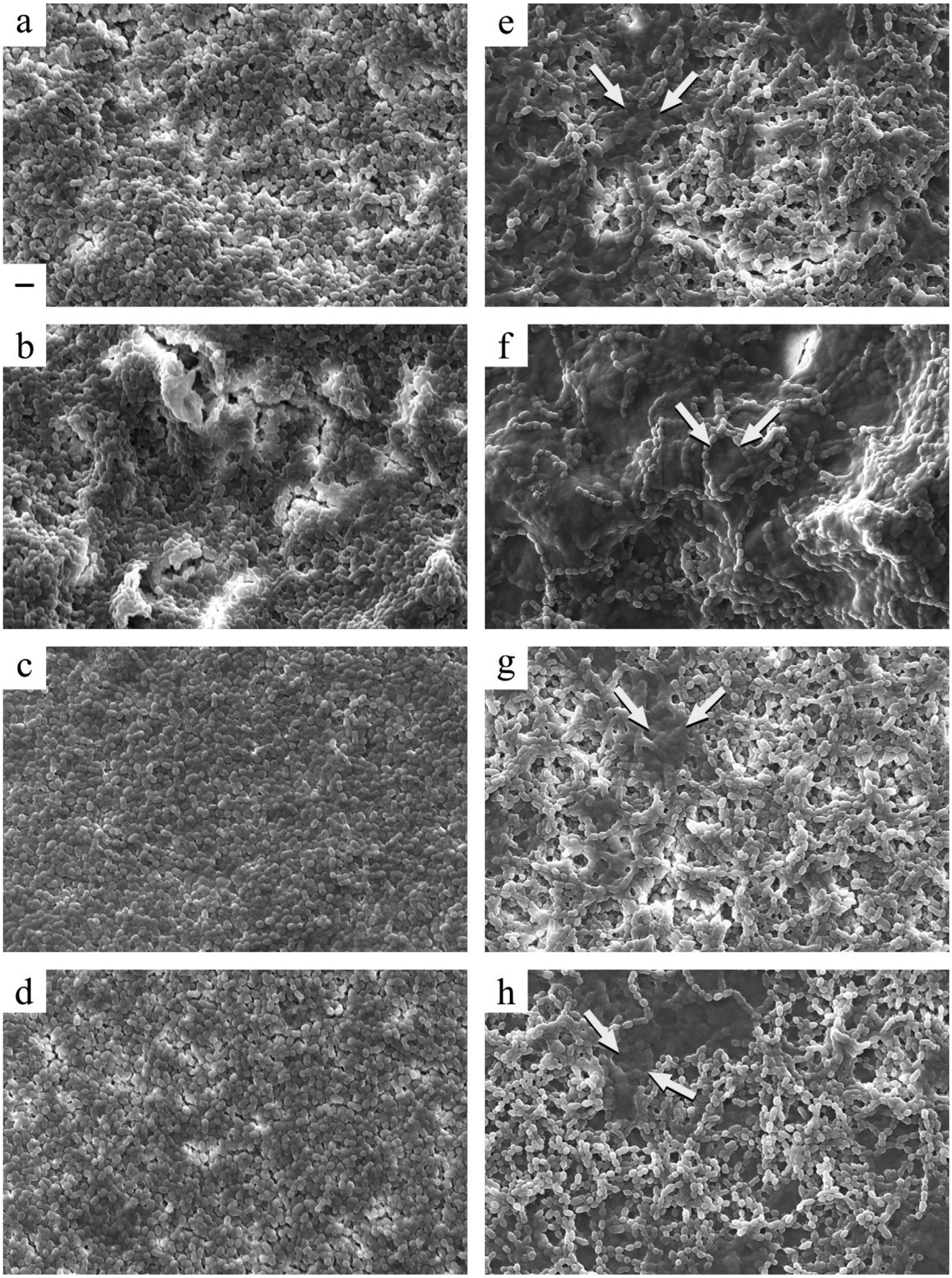

Fig. 14. *Streptococcus sanguinis* biofilms on various surfaces. (a-d) shows 72-h development, and (e-h) show 120-h development. Each row represents one material, top to bottom: PEEK, blasted PEEK, titanium, TiAlV alloy. Arrows indicate EPS-like substance around the streptococci. Scale bar shown in panel (a) represents 2 μm in all panels. Figure adapted from [228].

[49]. Zeta potential provides a more reliable indicator of a surface susceptibility to attachment than surface contact angle [256,257]. Particles are more prone to adhere to high-surface-energy metallic surfaces than low-surface-energy polymers [258]. However, there are always exceptions; studies report that an increase in the surface energy of substratum may lead to anti-fouling while others showed no correlation [245]. An increase of surface energy of helium- and oxygen-treated PET results in adherence reduction of *S. epidermidis* [259,260], which is known to be hydrophilic [261] and a cause of infection when adhered to surfaces in medical devices [246]. The treatment of titanium alloys with ultraviolet irradiation is shown to increase surface free energy and be anti-fouling to *S. epidermidis* [262].

The surface energy of solids theoretically divided into components [263] including an apolar Lifshitz-van der Waals force (γ_2^{LW}) and a polar Lewis acid-base force (γ_2^{AB}) [245]. The acid-base component is comprised of an electron acceptor (γ_2^{+}) and donor (γ_2^{-}). These two components are the main parameters that control bacterial adhesion to surfaces in the extended DLVO (x-DLVO) theory. In addition, the lower the strength of the electron donor (γ_2^{-}), the less bacterial adherence occurs as the electron acceptor (γ_2^{+}) in typically zero for most solid materials [264]. Accordingly, the ratio $CQ = \gamma_2^{LW}/\gamma_2^{-}$ [245,265] relates the surface energy component of Lifshitz-van der Waal (γ_2^{LW}) to the electron donor (γ_2^{-}) to investigate the discrepancies in the influence of surface free energy on bacterial adhesion. A variety Nickel-Phosphorus-Polytetrafluoroethylene (Ni-P-PTFE) composite coatings demonstrate a strong positive correlation between CQ and bacterial attachment.

A combination of low surface energy materials with patterned surfaces leads to a 21st century surface property known as 'superhydrophobicity' [266]. Such surfaces were initially inspired from nature and known for their ability to preclude bacterial adhesion [247,267]. The lotus leaf is the classic example of naturally inspired anti-fouling surface [268]) that possesses a high water contact angle, 170° [269], and self-cleaning property due to the hierarchical structured surface and low surface energy of the wax layer coating the leaf [270]. An implementation of such surfaces for anti-fouling has been demonstrated in the form of polymer coating stainless steel to resist two pathogenic bacterial strains, *P. aeruginosa* and *L.monocytogenes*, that arise in food processing and medical environments [271,272]. Superhydrophobic surfaces have also been shown to mitigate the risk of blood coagulation as demonstrated by reduction of bacterial adhesion to the inner surfaces of the blood vessels resulting from nitric oxide release [273].

3.2. Substrate material and topography, and biofilm growth

Surface topography, such as regular patterns and irregular roughness, dictates the success of bacterial defilement of substrates, which is also highly species-specific [39,49,184,211,256,274–279], as catalogued in Table 2, and schematized in Fig. 15. Nano-roughness (Fig. 15A-2) imposes a greater energy barrier to the incoming bacterial cells when compared to smooth (Fig. 15A-1) and micro-rough (Fig. 15A-3) surfaces, thereby promoting anti-fouling. Additionally, the contact pressure exerted by nano-pillars is sufficient to rupture the bacterial membrane, as schematized in (Fig. 15B-2). Bacterial cells secrete proteins that form a thin film to enhance the abililty of a surface to accept foulers by creating a chemical gradient. In the case of high aspect ratio nano-rough surfaces, protein particles seep through the pores which prohibits protein film formation, thereby reducing effective bacterial attachment, as shown in Fig. 15C-2. Micro and nano-rough surfaces produce local vortices near the surface as a result of the shear layer formed by bulk flow [280]. These local instabilities reduce fouling of micro and nano-rough surfaces compared to smooth surfaces, as schematized in Fig. 15D. Rough surfaces can entrap air between ridges that restrict bacteria from accessing the surface, as shown in Fig. 15E. Cell segregation is required for bacteria to form biofilms. Pores smaller than the smallest dimension of bacteria cells prevent segregation, hence promoting anti-fouling, as schematized in Fig. 15F. However, if the aspect ratio of the nano-roughness approaches unity, protein molecules can fill the pores essentially transforming the surface in to a smooth surface, as shown in Fig. 15G-2. In short, the influence of surface roughness is scale and situation dependent. Nano-roughness generally promotes anti-fouling while micro-roughness tends to aid fouling. Direct correlation between the surface roughness of a glass coupon and the adhesion rate has been demonstrated for the several bacterial

Table 2
Influence of surface roughness on bacterial attachment.

Surface material	Roughness [μm]	Influence on Attachment	Microorganisms	Reference
Titanium implant	0.81 and 0.35	25 times more bacteria attached to rougher surface	*Indigenous oral microbiota*	Bollen et al., 1997 [281]
Stainless steel with different surface finishes	0.009–0.145	Higher attachment on rougher surface	*Indegenous bacteria from poultry rinse*	Arnold and Bailey, 2000 [282]
Stainless steel	0.03–0.89	Higher attachment on rougher surface, bacteria tend to align with scratches of similar dimension	*P. aeruginosa, P. putida, D. desulfuricans, Rhodococcus spp.*	Medilanski et al., 2002 [283]
	0.01–1	No statistically significant difference	*S. thermophilus*	Boulange-Petermann et al., 1997 [284]
	0.5–3.3	No difference	*S. thermophilus, S. waiu*	Flint et al., 2000 [285].
	0.66–1.2	No difference	*L. monocytogenes*	Tide et al., 1999 [286]
	0.1–0.9	Smoothest surface had 100 times lower attachment than roughest surface, but the difference was minimal for hydrophobic strains	*P. aeruginosa*	Venhaecke et al., 1990 [287]
Polymethyl methacrylates	0.07–3	Reduction in roughness reduced adhesion	*S. sanguinis*	Dantas et al., 2016 [288]
Fluorinated glass	0.05–5	Attachment increased with micro-roughness but reduced with nanoroughness	*E. coli*	Encinas et al., 2020 [289]
Glass microscope slides, as is and etched with a buffer solution of hydrofluoric acid	0.0048–0.0122	3 times higher attachment on the smoother surface	*P. issachenkonii*	Mitik-Dineva et al., 2008 [290]
Glass microscope slides, as is and etched with a buffer solution of hydrofluoric acid	0.0048–0.0122	43% higher attachment on smoother surface	*A. fischeri*	Mitik-Dineva et al., 2009 [291]
		73% higher attachment on smoother surface	*C. marina*	
		18 times higher attachment on smoother surface	*S. flavus*	
		134% higher attachment on smoother surface	*S. guttiformis*	
		62% higher attachment on smoother surface	*S. mediterraneus*	
Titanium, with and without mechano-chemical finishing	0.00059–0.00112	2 times higher attachment on smoother surface	*S. aureus*	Truong et al., 2010 [292]
		6 times higher attachment on smoother surface	*P. aeruginosa*	

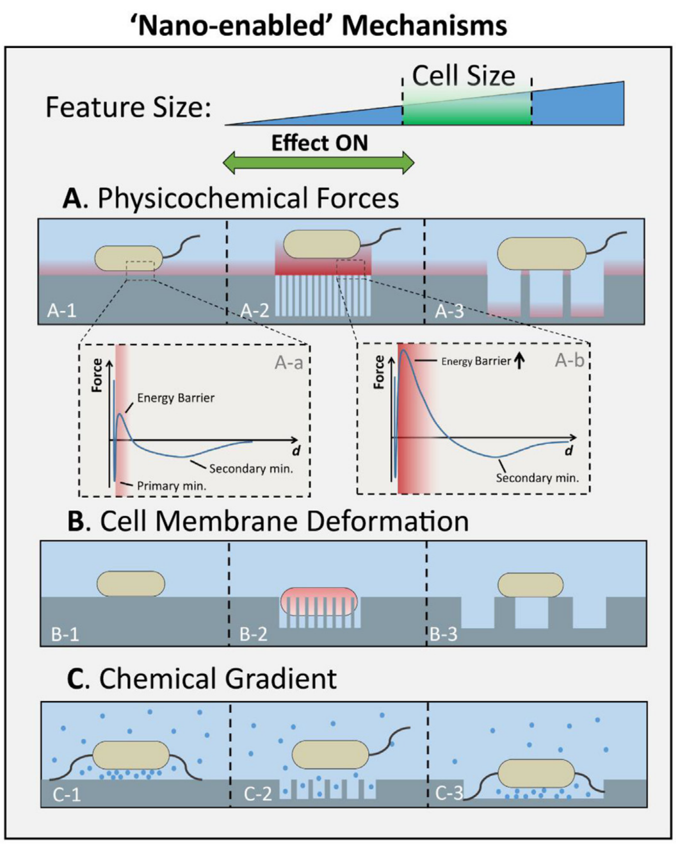

Fig. 15. Repelling effects of stratum topography on initial cell attachment, and their relevant scales. Panels (a-c) depict interactions augmented by surface features which are significantly smaller than a bacterium. Panels (d-g) illustrate the affect of features that are of the same scale as the cell, or larger. Each row shows, from left to right: flat, nanoscale, and microscale surface topographies. Figure from [274].

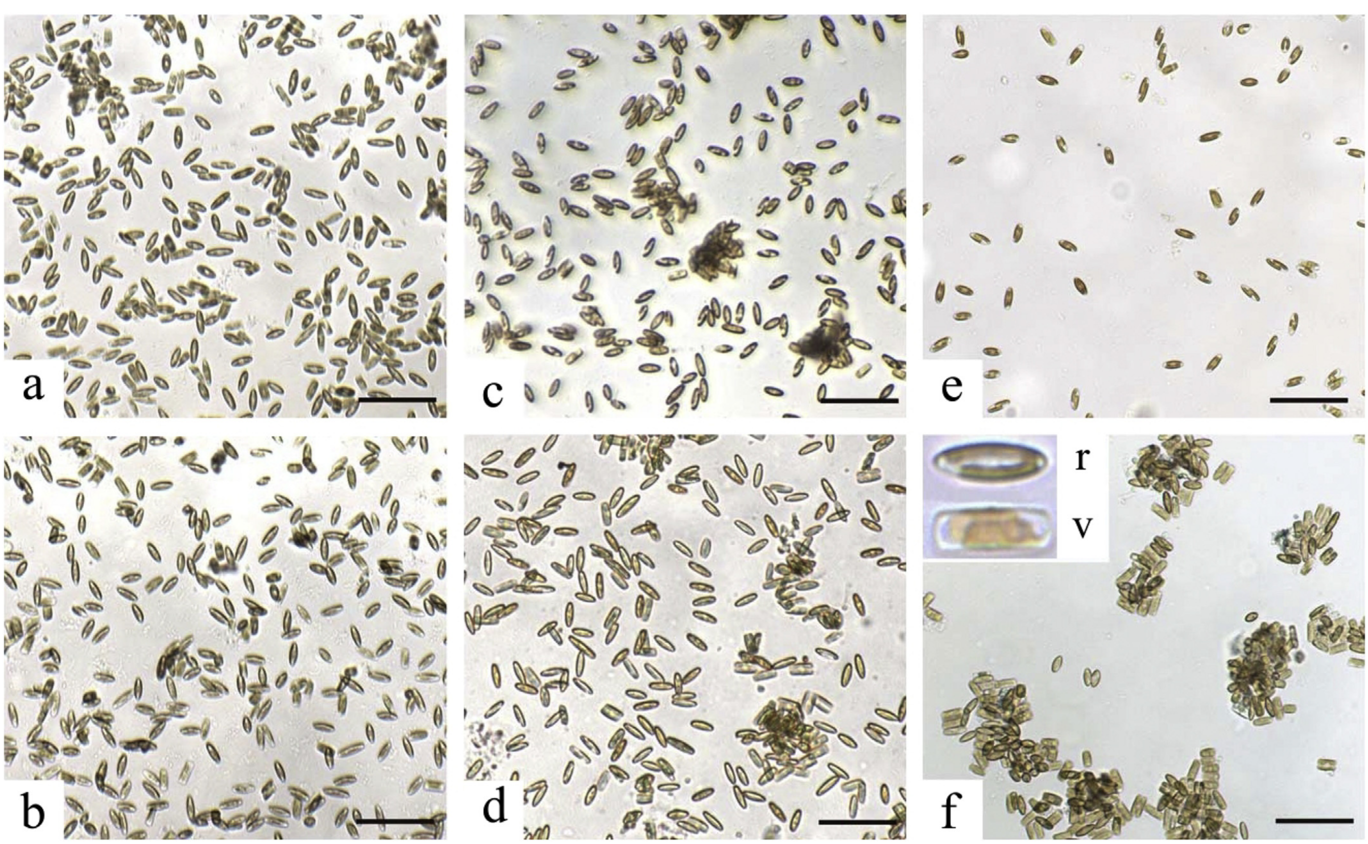

Fig. 16. Diatom biofilms cultivated on glass and polydimethylsiloxane elastomer (PDMS). Top row, (a,c,e) shows glass slides, bottom row, (b,d,f), PDMS slides. Testing channel hydrodynamic conditions are: (a,b) static medium, (c,d) shear stress of 0.54 Pa, (e) shear stress of 1.0 Pa, and (f) shear stress of 2.0 Pa Panel (f) inset illustrates the differences in cell arrangement: (r) raphe-side down orientation, (v) valve-side down orientation. Scale bars represent 50 μm. Figure adapted from [184].

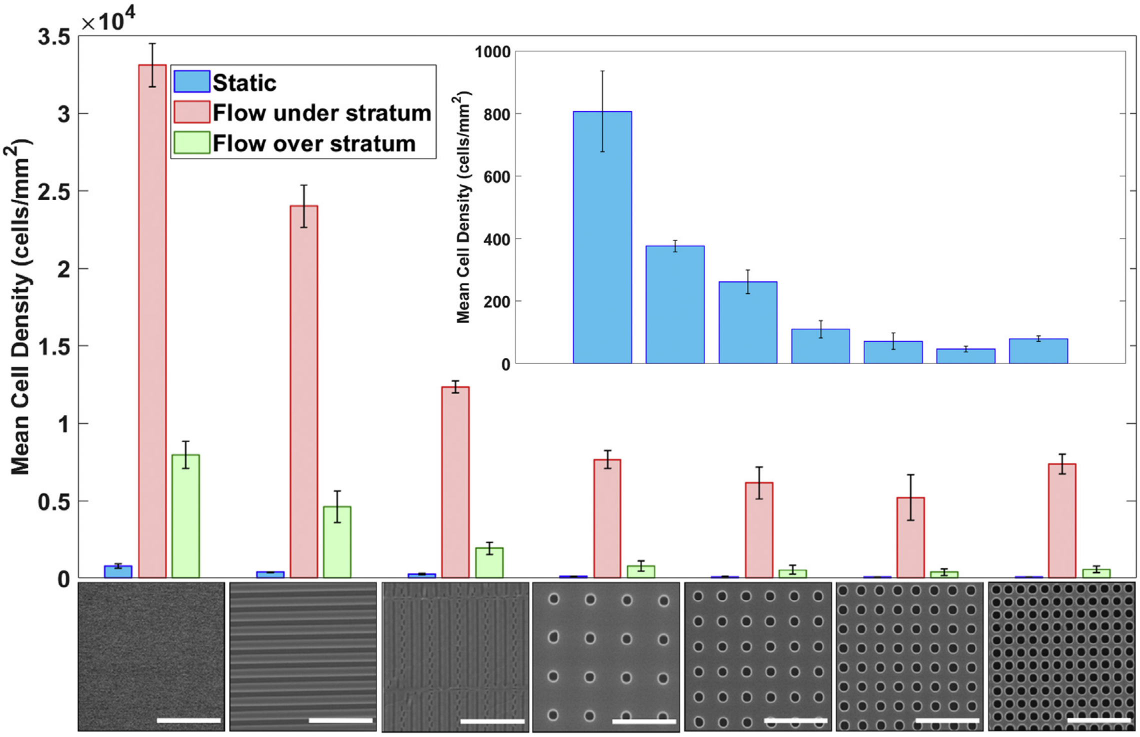

Fig. 17. Cell attachment to various PDMS surface topographies under (blue) static conditions, and in relation to stratum orientation during fluid flow: flow under stratum (red), and flow over stratum (green). The inset shows a zoomed view of the cell attachment on various surface topographies under static conditions. The x-axis shows the seven different surface topographies, from left to right, smooth surface, surface with continuous lines of 1 μm width and spacing, staggered lines of 230 nm line width, 4 μm spaced holes, 2 μm spaced holes, 1 μm spaced holes, and 0.5 μm spaced holes. All holes are 1.7 μm in diameter. The inset has the same x-axis. Error bars represent one standard deviation. Scale bars = 10 μm [49].

species, with the rate increasing five and ten times for the same increase in roughness [256].

Identical flow conditions can spawn a variety of biofilm growth characteristics dependent on the topography of the surface to which the biofilm is attached, as discussed in §2.2. For example, a shear stress of 1.3–1.4 Pa restricts biofilm growth on glass, but on PDMS biofilms continue to grow even at a shear stress of 2.0 Pa, as shown in Fig. 16 [184]. Furthermore, most of the cells will face the surface with their raphe-side on glass, but will face the stratum with valve-side down on PDMS (Fig. 16r, v). Compared to the smooth surfaces, the patterned surface of the PDMS decreases the cell retention. Under a wall shear stress of ~2 mPa, patterned PDMS surfaces are covered by an order of magnitude fewer cells compared to smooth surfaces [49], shown by the bars in Fig. 17. Static fluids typically result in lower cell attachment rates to the patterned surface, as shown in the inset of Fig. 17 [49]. Another interesting but counter-intuitive result of the study from which Fig. 17 is derived is that cell density on the surface over the flow is greater than that on the surface beneath the flow, a 4× disparity for a smooth surface and >10x for micro-porous surfaces. However, micro-pore spacing has little effect on the cell density, provided surface orientation remains the same. Anti-fouling via surface patterns is more effective when pattern shapes are engineered to mismatch the natural shape of the bacteria. Linear patterns, for example, attract more *E. coli* cells than circular-patterned arrays, indicating that circular shapes do not allow *E. coli* to fit within curved boundaries. The anti-fouling consequence of cell-pattern mismatch is illustrated by ability of the *Sharklet AF*™ pattern [293], biomimicked from sharkskin to resist fouling by *Ulva* alga. Sharkskin anti-fouling is attributed to three key factors: (i) pattern spacing that precludes cells from fitting within the pattern; (ii) pattern size that precludes cell stabilization on a single feature; and (iii) pattern topography, or depth, that precludes a resting cell from reaching the bed of the feature [275,276]. In creeping flow conditions, microscale confinement features have also been shown to inhibit biofilm formation through the formation of secondary flows within the semi-confined structures [280].

Some biological surfaces, such as those of lotus leaves, decrease affinity to fouling via entrapment of air on the microscale between epicuticular wax kernels [294]. Such properties serve as a guide for engineered treatments, where careful manipulation of topographies and roundness of surface textures can produce hydrophobic surfaces. Greater hydrophobicity and curvature thus promotes anti-fouling [295]. However, the impact on hydrophobicity should be considered in conjunction with surface tension. In cases where the surface tension of the medium is larger than that of bacteria, hydrophobic surfaces can attract bacteria [296]. In certain tests, hydrophilic surfaces had a lower rate of the attached cells, a correlation maintained across an increase in the ionic strength of the liquid medium [257].

The engineering of contact area topography must be executed in concert with careful consideration of surface chemistry. Experiments with polyethylene glycol (PEG)-silane grafted onto a nano-tubular patterned TiO_2 surface demonstrate that bacterial count does not scale linearly across the range of different pattern sizes, for neither coated nor uncoated surfaces, [277]. Regular surfaces would, as expected, be more susceptible to swarming compared to ones with micro-patterns, but less compared to ones with nano-patterns [278]. Between two hollowed substrates, the one with a pore size of 20 nm fouls more than the 80 nm pore channels, as shown in Fig. 18a [277]. Tests on structure-free dense TiO_2 surfaces (DT), nanotubular TiO_2 surface with pore size of 20 nm (TN20), nanotubular TiO_2 surface with pore size of 80 nm (TN80), and their PEG-treated variants (-P) reveal that fewer voids increase available contact area for attachment. A balance between the accessible surface area and surface friction forces can produce unwanted results, as shown in an example of PEG coating applied to a surface with 20-nm pores. Despite the PEG having biofouling resistant properties, the patterned substrate showed higher volume of attachment than the smooth surface coated with PEG, Fig. 18a. The effects of

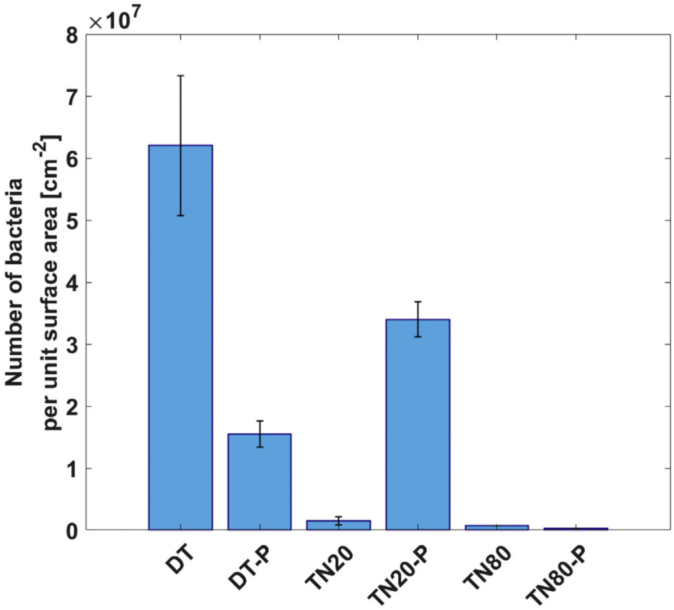

Fig. 18. *S. aureus* quantities on TiO_2 surfaces with various coatings. [277].

PEG coating are attributed to the higher friction coefficient of the patterned surface, which effectively reverses the advantage of a smaller contact area, Fig. 18b [277]. The results demonstrate that treatment of anti-fouling surfaces should account for multiple characteristics of engineered patterns.

While engineered, patterned surfaces discourage microorganism attachment, randomly increasing the surface area can produce opposite effects by facilitating microorganism attachment. Adverse phenomena of microbiologically influenced corrosion (MIC) has been observed in seawater transport pipework where bacteria settle in welds due to the random and locally increased roughness of the welds [279]. Furthermore, when observing a biofilm growth on a family of chemically similar materials (PP, PVC, HDPE, etc.) the inherent differences in material surface roughness are directly correlated to biofilm growth rates under otherwise identical flow conditions [183]. In simulated marine environments terrestrial animal fur demonstrated a promising level of resistance to algae fouling [297]. Fur density, length, and uniform arrangement promoted anti-fouling, indicating anti-fouling properties are superior for arrangements that resemble a patterned surface. We discuss hair and hair-like structures in greater detail in §3.5.

3.3. Substrate material and topography, chemical signaling, and detachment

Factors that initiate detachment are not fully understood, but seem to be based on chemical signaling that initiates release of cells following colony saturation and starvation [129,208,298,299]. Once the biofilm reaches maturation, bacteria purposely detaches from the surface in an effort to leave saturated biofilm colonies, reach more nutritious surroundings, and subdue new domains. This step is again affected by the characteristics of the substrate material [146]. An understanding of attachment mechanisms is precursory to comprehending detachment. Most microorganisms can irreversibly attach only after a short period of reversible or unsteady attachment [300]. However, cells that do connect with the surface will continue to rotate appendages and detach after a short time. The continued use of appendages after contact is an indicator of reversible attachment. Experiments with *Caulobacter crescentus* swimming between glass plates showed this process is quite swift: 68% of the cells attached within the first minute, and the remaining did so within the following four minutes [301]. *E. coli* and *Vibrio cholerae* first spread their flagella and use pili in combination with outer membrane proteins to anchor to the surface. *P. aeruginosa* need TfP to execute twitching motion on a surface and for subsequent buildup of a stagnant biofilm [129].

Once biofilms reach a mature stage they detach to explore other nurturing surfaces. At this point in the biofilm life-cycle, the cell count has increased dramatically compared to the initial reversible attachment phase. While the absolute number of detached cells also increases, as expected, the rate of detachment progressively slows[302]. With time, adhesion to both the surface and neighbouring cells strengthens, increasing the likelihood bacteria remain on the surface. Therefore, individual cell detachment is affected by the status of adjacent cells and the adhesion capability of the colony. As previously explained, the 'slingshot' mechanism of detachment is an efficient mechanism of transportation for TfP equipped bacteria [108], and cell orientation affects the irreversibility of the attachment. The majority of TfP equipped bacteria uproot themselves into a vertical position (Fig. 5b) before detaching from the surface. Those which remain at rest horizontally, or are otherwise unable to erect themselves, remain permanently attached [303].

As described in §3.2, the shape and scale of the surface crevices directly influence the attachment success. The same is true for detachment–materials with more diverse micro-topography, such as wood, retain microorganisms more readily than, for example, smoother plastic surfaces. However, if the surfaces of two different materials are treated in a similar manner, the difference in quantity of dislodged bacteria all but disappears [304]. An example of bacteria retention in pores that match the bacterial dimensions is shown in Fig. 19. Bacteria larger than an opening can only attach to the adjacent surface [49], Fig. 19a, but can lodge within crevices larger than the cell, Fig. 19b. Partial insertion occurs in the openings which are approximately the same size as the cell, as seen on Fig. 19c. Inserted cells increase the chances of retention under flow if the cell shape matches the shape of the opening. Shape similarity allows cells to align with the opening and increase the surface contact area, therefore increasing the force required to dislodge the cell [283]. Forceful removal of embedded foulants depends on the manipulation of force direction and the intensity [97,205]. The higher the applied force, the greater the removal effectiveness. More so, any use of mechanical force not only assists the cell removal process, but also increases the effectiveness of the disinfectants [207]. Application of mechanical force can also have adverse effects under special hydrodynamic conditions. For example, the formation of aerosols during a cleaning process facilitates spreading of the cells. In those cases, use of alternative methods such as a turbulent stream in an enclosed volume or conduit is required to subvert the risks of foulant spreading [205].

3.4. Modeling attachment and detachment of bacterial adhesion

The adhesion of bacteria to a substrate can be analyzed thermodynamically to ascertain the spontaneity of the adhesion/detachment process, done by using either a surface thermodynamic approach or DLVO theory and its extension, x-DLVO theory [59,306]. The surface thermodynamic approach compares interfacial free energy of the attracting surfaces with different liquids by measurement of liquid contact angles with the substrate and macroscopic bacteria lawns (bacterial colonies on surface). Contact angles permit the evaluation of critical expressions such as the equation of state, and energies arising from Lipschitz-van der Waals and acid-base interactions [307]. These interactions are key components of the thermodynamic free energy commonly expressed as $\Delta G_{adh} = \gamma_{BS} - \gamma_{BL} - \gamma_{SL}$, in which, γ_{BS}, γ_{BL}, γ_{SL} are the surface free energy of bacteria-solid, bacterial-liquid, solid-liquid interface, respectively. Adhesion is favorable if $\Delta G_{adh} < 0$ [296].

The drawback of the surface thermodynamic approach, which assumes thermodynamic equilibrium has been established, implying reversible adhesion, is the exclusion of electrostatic interactions between contacting surfaces. DLVO theory addresses electrostatic

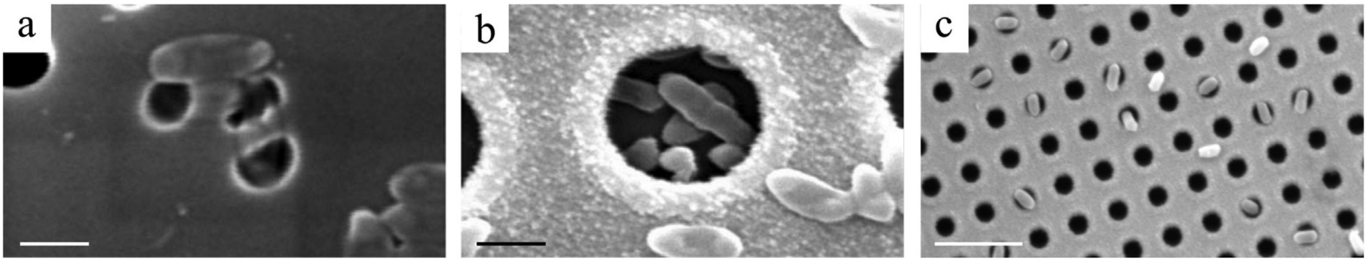

Fig. 19. Elongated *P. aeruginosa* cells on TiO_2 surfaces. Pore diameters: (a) 0.5 μm, (b) 2 μm, and (c) 1 μm. Scale bars represent 1 μm on panels (a) and (b), and 5 μm on panel (c). Panels (a) and (b) are from [305], and panel (c) is previously unpublished.

exclusion by framing the favorability of adhesion with the balance of two distinct short-range forces. The first, Lipschitz-van der Waals forces, are always attractive. The second is the repulsive energy due to electrostatic forces from the electrical double layer [308]. x-DLVO theory is required when repulsive forces are strongly dependent on pH and ionic strength of the solution [309,310]. x-DLVO includes acid-base interactions that measure the degree of hydrophobicity or hydrophilicity [311]. The total interfacial free energy, which is usually presented as a function of the separation distance *r* between the bacteria and substrate, is expressed as $\Delta G_{\text{int}}(r) = \Delta G_{\text{LW}}(r) + \Delta G_{\text{EL}}(r) + \Delta G_{\text{AB}}(r)$. The energy due to van der Walls forces, ΔG_{LW}, can be calculated between two surfaces by $\Delta G_{\text{LW}}(r) = -\int_{V1} dv \int_{V2} C\rho_1\rho_2 r^{-6} dv$ where V_1, V_2 are the enclosing volumes of the surfaces, *C* is a material-dependent constant, and ρ_1, ρ_2 are charge densities (e.g. atoms or molecules per unit volume). The expressions for general surface shapes require numerical methods, but for simplified geometries, closed form expressions are possible [312]. The repulsive electrostatic energy $\Delta G_{\text{EL}}(r)$ requires the measurement of zeta potentials for interacting surfaces, typically obtained using the Debye-Huckel Eq. [313]. The approximate analytical expressions for acid-base interactions available in literature [307,314] between a flat surface and a sphere of radius *R* (a good approximation of a bacteria near substrate) is given by $\Delta G_{\text{AB}}(r) \approx 2\pi R h_0 \Delta G_{\text{H}}^0 \exp\left[(H_0 - r)/h_0\right]$. Here, ΔG_{H}^0 is an energy density constant term representing the polar component of the surface tension obtained from contact angle measurement between bacteria and substrate [315]. The minimum distance at which the two surfaces (sphere and plate) approach each other is $H_0 \approx 0.163$ nm [316], and h_0 is the decay length of water which does not change significantly with ionic strength [317]. For the case of hydrophilic repulsion, the decay length is frequently 0.6 nm but can be as high as 13 nm for hydrophobic attraction [317]. The computed energy landscapes reflect the nature of potential wells and barriers along the separation coordinate and positively correlate with the success of the initial approach stage. Higher potential barriers require greater kinetic energy during the approach of bacteria to a surface. Multiple wells (secondary minima) may indicate available stable positions at a distance from the substrate, indicating bacteria are trapped away from the surface. Detachment forces can be computed from the spatial gradients of free energy.

The above approaches do not consider the effect of localized deformation of neither the bacteria nor the substrate. When deformation is appreciable, elastic energy must also be considered [318]. A comprehensive record of approaches that cope with surface deformation can be found in classical contact mechanics of adhesion literature, which rely on a continuum description [319]. The most commonly used theory between a moderately compliant sphere and flat surface is the Johnson-Kendall-Roberts (JKR) model that assumes small strains with only surface adhesive energy and neglects explicit surface tension. JKR theory predicts a detachment force of $F_{\text{detach}} \approx 1.5\pi R\gamma$ where γ is surface adhesive energy. When the sphere is rigid compared to the substrate, the Derjaguin-Muller-Toporov (DMT) model is more precise and gives $F_{\text{detach}} \approx 2\pi R\gamma$. The detachment process in the presence of large localized deformation is considerably more complicated, requiring information on material nonlinearity and large deformation kinematics [320]. In addition, if the elastic modulus of the deforming bodies is small compared to surface tension, the role of surface tension becomes critical in the detachment [318]. The dominance of surface tension can be estimated using the elasto-capillary length $\ell_{\text{ec}} = \sqrt{G/\gamma_S}$ where *G* is shear modulus, γ_S is surface tension. If the characteristic length of the deformation is higher than ℓ_{ec}, surface tension effects become significant.

The kinetics of bacterial detachment from a substratum are dependent on the residence-time of bacteria on the surface [321,322]. The residence time $(t - \tau)$ is defined as the difference between the desorption time *t* and the time τ at which the bacteria arrives at the surface. The desorption rate $\beta(t - \tau)$ of individual bacteria can be microscopically monitored by capturing images when bacteria approaches the bottom surface of a parallel plate flow chamber [321]. Image analysis allows for distinction between moving and adhering bacteria. The desorption rate was found to exponentially decay as a function of the residence-time, $\beta(t - \tau) = (\beta_\infty - \beta_0)\exp\left[-(t - \tau)/\tau_c\right]$ [321,322] where β_0 and β_∞ are the initial and final desorption rate coefficients, and τ_c refers to the characteristic residence time. The adhesion strength between the bacteria and substratum weakens when $\beta_0 < \beta_\infty$.

Empirical models can also be obtained using the atomic force microscopy (AFM) which is a promising technique for characterizing the bond strengthening time-scale of adhered bacteria. Bond strengthening occurs because the adhesive bond between bacteria and substratum strengthens over time; the forces needed to prevent adhesion are smaller than the ones needed for detachment [323]. The measurement of adhesion forces through AFM is performed via analyzing the 'retract force-distance curve' taken at various different surface delay times, which is the time at which the adhesion forces are strengthened. The forces of adhesion were observed to increase exponentially before reaching a plateau [323] according to $F(t) = F_\infty + (F_0 - F_\infty)\exp\left[-t/\tau_k\right]$ in which F_0, F_∞ refer to the initial maximum adhesion force and the maximum adhesion force after bond maturation, respectively, while τ_k is a characteristic time needed for strengthening the adhesion force.

The above theories provide detachment characterizations under ideal conditions. In reality, the bacteria-substrate system can be subjected to a complex set of biophysical forces arising from interface chemical changes, and local biological growth and secretion. These factors intimately depend on the combined action of bacteria, interface and surrounding media, and modeling them accurately can be a formidable challenge. Finally, these models also assume that the nature of interface constitutive behavior is relatively unaffected by far-field variables, in which case the detachment forces can be treated as boundary conditions and linked to the overall continuum behavior using appropriate balance laws. The resulting equations provide the various critical hydrodynamic, material and geometrical variables corresponding to the detachment process.

3.5. Fouling of hair-like structures

A promising path forward in anti-fouling strategies may be further exploration of natural solutions to fouling by both mechanical and chemical means [11,324,325]. While the anti-fouling properties of numerous flora and fauna have been explored in regard to surface topography, the role surface deformation plays in self-cleaning is underexplored. Animals do not provide static environments in which most foulers are found and have the ability to actively clean parts of their bodies. Insects and mammals have the ability to rid their bodies of accumulated moisture through high acceleration [326–328], shaking and vibration, and thus rid their bodies of conditions friendly to fouling. Such behaviors may also be effective at removing inorganic foulants such as dirt and debris. The inability to self-clean would hinder the ability of an animal to locomote [329], repel water [330,331], or regulate body temperature [332,333]. Semi-aquatic mammals are of particular interest because despite the available provisions for microorganism proliferation and the frequency of submersion, their furs escape the burden of biofouling. The anti-fouling nature of fur has been previously observed [297] but physical characterization remains undone. In general, biofouling on surfaces which can significantly deform is poorly understood.

Biofouling of hair-like surfaces is essentially multi-scale in nature with intricate fluid-structure interactions. At the lowest and most fundamental length-scales stands the problem of fouling single hairs whose deformation takes place at relatively low diameter Re. Further complication is introduced by the aggregate structure of fur, creating a larger relevant length-scale. Here, fouling at the fur patch length-scale can be viewed as emergent from the collective behavior of individual hair strands. The Re at different length-scales gives rise to different fluidic loads and thus the overall behavior is expected to be a function of numerous fur length-scales, fur packing density in a patch, fluidic flow rates, and physiology of the fouling organism. At the smallest scale fouling will depend on fur surface chemistry and topography. Due to the multi-scale nature of the fouling process, the role of such microscopic features propagates to the larger scales. The mechanisms through which deformation and deposition can occur is understudied.

A simple model of quiescent flow is described herein in an early attempt to describe the role of deformation and surface topography on the fouling process. External fouling transport is assumed to be diffusive in nature. The steady-state diffusion of the external fouling transport is modeled by the Laplacian, $\nabla^2 C = 0$ in an infinite domain Ω surrounding the fur. The deposition kinetics of bacteria along the fur surface are assumed to take a flux type boundary condition (first-order reaction law). The flux q on the surface of fur, Γ, is expressed as $q = \partial C/\partial n = k(C - C_0)$. Here k is the adsorption rate of bacteria, C is the surface concentration, and C_0 is an empirical constant characteristic of the surface. Further assumptions include the concentration at infinity to be fixed at $C = C_\infty$, simulating a reservoir of bacteria.

The role of topography and fur deformation on deposition kinetics can be elucidated via treating the fur as a beam-like structure inside an infinite media with topography on only one side. To this end, a select case with length L=1 and thickness $h = 0.01$ cm is used for illustration. The topography is presented in the form of overlapping 20 scale-like plates with thickness $D = 0.005$ cm and inclination angle of $\theta_0 = 6^\circ$. The scales are dense so that the distance between scales, which defines the overlap ratio, is approximately zero. Without loss of generality, the boundary conditions are assumed as $C_\infty = 10$, $k = 1$ and $C_0 = 0$ leading to $q = C$ on Γ. Since the domain outside the fur is assumed infinite, the solution of the Laplacian equation is obtained by the boundary element method (BEM) [334,335], as a traditional finite element (FE) method would require meshing infinite size domains. The BEM results are validated with a few test cases using a commercial Finite Element (FE) software assuming a very large external domain.

For this case, the concentration (normalized by the concentration at far-field) along both surfaces of the fur (smooth/topographic) can be seen in Fig. 20a. Topography along the surface leads to reduced concentration and mass deposition per unit area compared to the flat smooth surface. Such results are completely altered once the surface is deformed. For example, when the fur is assumed to be initially deformed according to $y(x) = A \sin \pi x$, $A = -0.1$ and $x \in [0\ 1]$, the concentration of bacteria varies significantly along the smooth and topographic side, Fig. 20a. Interestingly, the smooth side of the curved fur is found to accumulate more mass along the surface compared to smooth-flat. However, the opposite is true for the topographic side, implying bacteria tend to travel far from topographic convex surfaces. The role of convex and concave curvature along with topography is presented in Fig. 20b, illustrating the steady-state mass deposition rate per unit length along the surface $M_t = \int_{LS} q dS / L_S$ versus curvature (convex to concave), where dS refers to a line element for either the topographic or smooth surface and L_S is the total arc length of the surface. Mass deposition rate is reduced with convex curvature. Particularly, topography along the convex curvature is observed to reduce mass deposition rate per unit length along the edge. In addition, the density of topography can significantly affect deposition rate per unit length as shown in Fig. 20b for the case of 10 and 30 scale-like plates on the top surface. There is not, however, a significant difference between the smooth sides for the two cases illustrated. Note that an increase in the concave curvature leads to settlement of the deposition rate per unit length, where curvature does not have any role in mass deposition rate along the surface. The same is not true for the case of convex curvature, where more curvature leads to more bacterial repellency. These preliminary results indicate that an interplay of the biofilm transport processes with deformation exists and point to an interesting frontier of investigation. However, much is sill unknown such as the bacterial interface adhesion mechanism and exact nature of surface adsorption kinetics which can dictate boundary conditions. Interestingly, rough topographies, especially if they are overlapping are known to produce highly intricate nonlinear and directional mechanical properties dictated by the topography [336–340]. Although there have been significant advances in biofilm evolution and formation simulations over the years [22,31,61,144,180,210], when coupled with fluidic loading, biofouling would be an exciting unexplored area of advancing computer simulations which can lead to the design of tailorable and tunable anti-fouling surfaces via topographic features and deformation.

4. Discussion and concluding remarks

Only by understanding fouling mechanisms may we generate effective anti-fouling strategies. The complex life-cycle of biofilms is governed by factors that can be broadly classified into genotypic, physio-chemical, stochastic, deterministic, mechanical, import-export, and temporal [23]. Hydrodynamics are often overlooked but determine if the aforementioned factors support or are a detriment to the proliferation of microorganisms. Bulk fluid flow influences growth rate [33,61–66], structure [33,55,67–70], shape [60,71–73], cell concentration [68,74–76], and detachment [16,22,77,78]. Biofilms are comprised of 80% cells held together by an EPS matrix with numerous zig-zag pathways and tunnels for nutrient and oxygen ingress [22,27,55,80]. While fluid flow promotes convection, sedimentation and diffusion are the primary forms of bacterial mass transport along surfaces in the absence of flow [33,52,53,55,59,88–92]. The role of hydrodynamics extends to both motile and non-motile microorganisms. While non-motile bacteria rely heavily on fluid flow, motile species display locomotion using their appendages in the absence of flow [16,18–20]. In both cases bulk flow aids cell transport toward surfaces to the proximity dominated by van der Waals and electrostatic forces acting across sub-millimetric length-scales [99]. Motile bacteria possess appendages, flagella and/or pili. Flagella enable initial reversible attachment to the surface, while pili ensure attachment becomes irreversible [5,38,96,103–106,108]. In contrast to laminar flow which produces thicker and less dense biofilms [51,52,55–57], the increased shear associated with turbulent flow

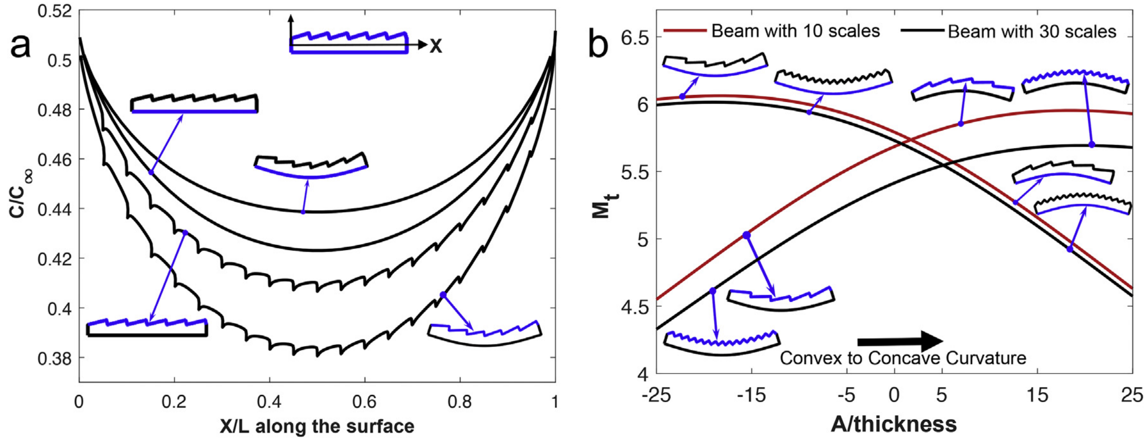

Fig. 20. (a) Normalized external fouling concentration along the smooth and topographic side of straight and deformed beam mimicking fur. (b) Steady-state mass deposition rate per unit length (cell/cm.s) along both (smooth and topographic) sides of a beam initially deformed in a sinusoidal shape at various deformation amplitudes.

promotes thinner but denser biofilms [53,54,57,58,60,62,78,119–121]. Although formation of filamentous streamers is associated with turbulent flow [73,162,163], streamers may form under laminar flow where secondary flow exists [20,71,72,156,173,176]. Streamer length can range from microns [71,167,171,172] and millimeters [20,162,168,173] in bacterial films, to several centimeters [56,151,152,174] in algal films. Streamer dislodgement clogs conduits [164] and micro-separation devices [166–168], increasing pressure drop and the associated energy costs of operation.

Upon maturation or encountering nutrient deficiency, biofilms detach and travel downstream either in parts or as a whole in search of a nutrient rich environment to inhabit [203]. In absence of protection from surface topography, a critical wall shear stress of 0.24 N/m^2 impairs the EPS generation and facilitates detachment [183]. Materials that succumb to biofouling range from PVC, cross-linked polyethylene, HDPE, PP [183,218–221], glass [222], PTFE [227], PEEK, blasted PEEK, commercially pure titanium, and titanium alloys [228] natural latex [225], cement, iron [201], and galvanized [223] and stainless steel [224]. Even though these materials are all susceptible to fouling, the extent of biofilm formation varies from material to material. Plastics like PET and PE typically support 50% of fouling biomass compared to steel and 63% of that on wood [229]. However, physical degradation of plastics decreases the resistance to biofouling, while biofouling enhances the degradation process [230,231]. Patterned surface topographies, if they are the same length-scale as the bacterial foulants, promote biofouling compared to smooth surfaces. However, if the length-scales of the surface topographies are orders of magnitude smaller than the fouling bacteria, the surface is more effective at anti-fouling [49,184,274–279]. The anti-fouling property of nano-rough surfaces can be attributed to several factors, such as increased contact pressure, decreased contact area, increased local vorticity, increased air pockets, and decreased chances of cell segregation [274]. However, the extent of fouling and anti-fouling ability of a surface is highly species-specific [341]. Anti-fouling via surface patterns is more effective when patterns are engineered to mismatch the targeted foulant species [275,276,293]. Textures that match a species promote attachment and retention while hindering detachment. In addition to carefully engineered surface topography, low surface energy restricts bacteria from fouling the surface. An optimal surface free energy of 20-30 mN/m is associated with minimum fouling by bacteria [247–250,252–254]. In general, engineering surface topographies is expensive and might not be cost effective for repelling multiple foulant species that present an array of shapes and sizes. Thus, a universal design of surfaces that is durable and capable of reducing bacterial biofouling for various types of bacterial strains and applications is likely impossible.

Biofilm cultivation utilizes a wide variety of flow systems, as described in more detail elsewhere [87,342]. The most common fluidic devices, repeatedly encountered within the scope of this review, can be classified into several broad groups. The simplest of the devices are nothing more than enclosed fluid conduits, either rectangular flow cells [60,132,343,344], rectangular channels [184,191], or circular tubes [200,221,345], equipped with a viewing port which allows for macro or microscopic observation of the biofilm. Where required, these devices are scaled down to form capillary flow cells [346] or microchannels [64,71,173,347,348]. The use of soft-lithography and related material manipulation techniques is useful when even finer topographic resolution is required, as is the case in microfluidic devices [212], micro pillar [72,168] or micro porous devices [157,349]. Continuous or batch cultivation of biofilms can be achieved in biofilm reactors. Commonly used reactors are rotating annular reactors [197,199,350] which allow control of the testing surface wall shear stress simply by modulating the angular velocity of the reactor. Other types of reactors include drip flow, rotating disk, and CDC biofilm reactors. The Robbins device is an inline flow type of a reactor, equipped with inserts that hold the testing samples flush with the conduit inner surface, allowing for easy removal of the coupons without the disruption of the biofilm ecosystem [112,207]. Marine and fresh water biofilm investigations sometimes do not require flow devices at all. The testing is conducted by simple immersion of tested materials in the flowing body of water [189,229]. New venues of investigation and phenomenon-specific challenges guide the researchers toward the development of novel flow chambers. Innovative designs are constantly introduced to enable investigations in which the more conventional devices cannot perform [211,351–356].

The effects of temperature on the biofilm life-cycle have been mentioned only as an additional factor governing biofilm proliferation (Table 1). Temperature variations exceed the scope of this review as they introduce complex biological transformations, such as changes in cell expression [357–359] or an increase in piliation [75,360,361]. In addition, the vast majority of the work discussed in this review has been completed at constant temperatures, typically established to provide optimal growth conditions for a particular species [221,223,225,362–364]. It is important, however, to note that temperature variations introduce similar effects to that of the other factors catalogued in Table 1. Such consequences include changes in EPS formation, attachment rate, probability of detachment, and viscoelasticity. Temperature variation is able to produce synergistic effects when acting together with other external factors, such as introduction of biocidal chemicals [19,27,75,207,365–367]. Temperature as a factor in biofilm removal is most relevant at the extreme values. Techniques such as autoclaving [368] or freezing [369] allow for significant biofilm removal, alone or in combination with other removal methods.

Biofouling research is an enduring topic that will continue to capture the attention of the scientific community due to the complex and highly situational nature of fouling. Despite the volume of fouling literature, there exist under-explored environments for which fouling is pervasive. Non-Newtonian fluids provide one such area that has received little attention with respect to biofouling despite blood expressing non-Newtonian behavior. Bacterial infections from temporary and permanent implants frequently contact non-Newtonian fluids. In §1 we note that biofilm communities have certain benefits but are under investigation predominately due to their detrimental impacts. The research discussed in this review enabled a variety of biofilm removal techniques, applied across different industries. The mechanical force of water or air jets is used in the dental industry to remove plaque biofilms [370,371]. Agitation of fluid suspended in the root canal is used as an effective cleaning method [372], and photon-induced photoacoustic stream (PIPS) increases the effectiveness of root canal disinfectants [373]. The synergistic effects of a high pressure spray are discussed in §2.3, for applications in the food industry [204]. Similarly, flushing of potable water pipework alone cannot remove the biofilm [374,375], but when combined with chlorination, flushing results in significant biofilm detachment [376]. A range of biofilm removal techniques relying on fluid flow are employed in water cooling plants as ecological alternatives to the use of chemicals [377]. Ultrasonically activated steam (UAS) generates bubbles in low velocity water, at 1–2 l/min, thus allowing in-situ removal of marine micro- and macro-foulants [378]. Selective surface textures promoting anti-fouling have been tested in the dental industry but increasing the complexity of the surface to repel biofouling needs to be a deliberate, engineered effort, rather than a stochastic increase in complexity. Synergy of existing engineered surface topography manipulation methods with chemical treatment and coatings may increase the effectiveness of fouling-resistant efforts. Biological systems often provide promising templates by which to engineer robust anti-fouling surfaces [11]. Outstanding examples are sharkskin and the lotus leaf, but the vast majority of natural surfaces remain uncharted in regard to anti-fouling capacity. Future researchers may, for example, choose to explore the anti-fouling mechanisms that lie within the skin and fur of aquatic and semi-aquatic species. In particular, organisms which reside at the air-water interface and do not foul may http://www.overleaf.com/project/5d3f070529de862c79d942faayprovide inspiration for decades of researchers.

Declaration of Competing Interest

The authors declare that they have no known competing financial interests or personal relationships that could have appeared to influence the work reported in this paper.

Acknowledgements

All authors except AK acknowledge NSF (CMMI-1825801) for funding this work. AK acknowledges support from DST-SERB (India). The authors thank Dr. Nathaniel C. Cady for bacterial surface attachment data and electron micrographs of surface topography (Fig. 17), Dr. Jacinta C. Conrad for the biofilm growth time-scale vector graphics (an input to Fig. 1), Kristen Griffin for permission to use the cell cluster oxygen gradients diagram (Fig. 7a), Dr. Minyoung Kevin Kim and Dr. Howard A. Stone for the image of channel network streamer formations (Fig. 10d), Dr. Cristian Picioreanu for the nutrients gradients model graphical output (Fig. 7b), Dr. An Rong for the fouling data for patterned TiO_2 surfaces (Fig. 18), Dr. Roberto Rusconi for the photographs and 3-D views of laminar flow streamers in zig-zag channels (Fig. 10b, c), and Dr. Kathryn Whitehead for the capture of bacteria lodged in a patterned surface (Fig. 19c).

References

[1] López HM, Gachelin J, Douarche C, Auradou H, Clément E. Turning bacteria suspensions into superfluids. Phys Rev Lett 2015;115:028301.
[2] Takatori S, Brady J. Superfluid behavior of active suspensions from diffusive stretching. Phys Rev Lett 2017;118:018003.
[3] Flemming H-C, Neu TR, Wozniak DJ. The eps matrix: the "house of biofilm cells". J Bacteriol 2007;189:7945–7.
[4] Flemming H-C, Wingender J, Szewzyk U, Steinberg P, Rice SA, Kjelleberg S. Biofilms: an emergent form of bacterial life. Nat Rev Microbiol 2016;14:563.
[5] Karimi A, Karig D, Kumar A, Ardekani AM. Interplay of physical mechanisms and biofilm processes: review of microfluidic methods. Lab Chip 2015;15:23–42 ISSN 1473-0197 https://doi.org/10.1039/c4lc01095g.
[6] Wilking JN, Angelini TE, Seminara A, Brenner MP, Weitz DA. Biofilms as complex fluids. MRS Bull 2011;36:385–91.
[7] Barai P, Kumar A, Mukherjee PP. Modeling of mesoscale variability in biofilm shear behavior. PLoS One 2016;11:e0165593.
[8] Ghosh T, Ngo T-D, Kumar A, Ayranci C, Tang T. Cleaning carbohydrate impurities from lignin using pseudomonas fluorescens. Green Chem 2019;21:1648–59.
[9] Badal D, Jayarani AV, Kollaran MA, Kumar A, Singh V. Pseudomonas aeruginosa biofilm formation on endotracheal tubes requires multiple two-component systems. J Med Microbiol 2020;69(6):906–19 [p. jmm001199].
[10] Chan J, Wong S. Biofouling: Types, impact and anti-fouling. Nova Science Publishers; 2010 [Incorporated].
[11] Bixler GD, Bhushan B. Biofouling: lessons from nature. Philos Trans R Soc A Math Phys Eng Sci 2012;370:2381–417.
[12] LoVetri K, Gawande PV, Yakandawala N, Madhyastha S. Biofouling and anti-fouling of medical devices. Biofouling Types, Impact Anti-Foul 2010:105–28.
[13] Camper AK, McFeters GA. Problems of biofouling in drinking water systems; 2000.
[14] Hellio C, Yebra D. Advances in marine antifouling coatings and technologies. Elsevier; 2009.
[15] Gordon DP, Mawatari SF. Atlas of marine-fouling bryozoa of New-Zealand ports and harbours. Miscellaneous Publication New Zealand Oceanographic Institute; 1992.
[16] Korber DR, Lawrence JR, Sutton B, Caldwell DE. Effect of laminar flow velocity on the kinetics of surface recolonization by mot+ and mot- pseudomonas fluorescens. Microb Ecol 1989;18:1–19.
[17] Rijnaarts HH, Norde W, Bouwer EJ, Lyklema J, Zehnder AJ. Bacterial adhesion under static and dynamic conditions. Appl Environ Microbiol 1993;59:3255–65.
[18] Scheuerman TR, Camper AK, Hamilton MA. Effects of substratum topography on bacterial adhesion. J Colloid Interface Sci 1998;208:23–33.
[19] Evans LV. Biofilms: Recent advances in their study and control. CRC press; 2003.
[20] Kim MK, Drescher K, Pak OS, Bassler BL, Stone HA. Filaments in curved streamlines: rapid formation of staphylococcus aureus biofilm streamers. New J Phys 2014; 16:065024.
[21] Wheeler JD, Secchi E, Rusconi R, Stocker R. Not just going with the flow: the effects of fluid flow on bacteria and plankton. Annu Rev Cell Dev Biol 2019;35:213–37.
[22] Picioreanu C, Van Loosdrecht MC, Heijnen JJ. Effect of diffusive and convective substrate transport on biofilm structure formation: a two-dimensional modeling study. Biotechnol Bioeng 2000;69:504–15.
[23] Wimpenny J, Manz W, Szewzyk U. Heterogeneity in biofilms. FEMS Microbiol Rev 2000;24:661–71.
[24] Stewart PS. Diffusion in biofilms. J Bacteriol 2003;185:1485–91.
[25] Fux CA, Costerton JW, Stewart PS, Stoodley P. Survival strategies of infectious biofilms. Trends Microbiol 2005;13:34–40.
[26] Wolcott RD, Rumbaugh KP, James G, Schultz G, Phillips P, Yang Q, et al. Biofilm maturity studies indicate sharp debridement opens a time-dependent therapeutic window. J Wound Care 2010;19:320–8.
[27] Rosenberg E, DeLong EF, Lory S, Stackebrandt E, Thompson F. The prokaryotes: Actinobacteria. Springer; 2014.
[28] Kumar A, Alam A, Rani M, Ehtesham NZ, Hasnain SE. Biofilms: survival and defense strategy for pathogens. Int J Med Microbiol 2017;307:481–9.
[29] Petrova OE, Sauer K. Escaping the biofilm in more than one way: desorption, detachment or dispersion. Curr Opin Microbiol 2016;30:67–78.
[30] Neethirajan, S., Karig, D. K., Kumar, A., Mukherjee, P. P., Retterer, S. T. & Doktycz, M. J Biofilms Microfluidic Dev.
[31] Picioreanu C, Van Loosdrecht M, Heijnen J. Discrete-differential modelling of biofilm structure. Water Sci Technol 1999;39:115–22.
[32] Wagner M, Taherzadeh D, Haisch C, Horn H. Investigation of the mesoscale structure and volumetric features of biofilms using optical coherence tomography. Biotechnol Bioeng 2010;107:844–53.
[33] Conrad JC, Poling-Skutvik R. Confined flow: consequences and implications for bacteria and biofilms. Ann Rev Chem Biomol Eng 2018;9:175–200.
[34] Radwan S, Al-Hasan R, Salamah S, Al-Dabbous S. Bioremediation of oily sea water by bacteria immobilized in biofilms coating macroalgae. Int Biodeter Biodegr 2002;50:55–9.
[35] Sarró MI, García AM, Moreno DA. Biofilm formation in spent nuclear fuel pools and bioremediation of radioactive water. Int Microbiol 2005;8:223–30.
[36] Singh R, Paul D, Jain RK. Biofilms: implications in bioremediation. Trends Microbiol 2006;14:389–97.
[37] Edwards SJ, Kjellerup BV. Applications of biofilms in bioremediation and biotransformation of persistent organic pollutants, pharmaceuticals/personal care products, and heavy metals. Appl Microbiol Biotechnol 2013;97:9909–21.
[38] Mattick JS. Type iv pili and twitching motility. Annu Rev Microbiol 2002;56: 289–314.

[39] Anselme K, Davidson P, Popa A, Giazzon M, Liley M, Ploux L. The interaction of cells and bacteria with surfaces structured at the nanometre scale. Acta Biomater 2010; 6:3824–46.
[40] Bjarnsholt T, Alhede M, Alhede M, Eickhardt-Sørensen SR, Moser C, Kühl M, et al. The in vivo biofilm. Trends Microbiol 2013;21:466–74.
[41] Persat A, Nadell CD, Kim MK, Ingremeau F, Siryaporn A, Drescher K, et al. The mechanical world of bacteria. Cell 2015;161:988–97.
[42] Sutherland IW. The biofilm matrix–an immobilized but dynamic microbial environment. Trends Microbiol 2001;9:222–7.
[43] Simoes M, Simões LC, Vieira MJ. A review of current and emergent biofilm control strategies. LWT-Food Sci Technol 2010;43:573–83.
[44] Subramani K, Jung RE, Molenberg A, Hämmerle CH. Biofilm on dental implants: a review of the literature. Int J Oral Maxillofac Implants 2009;24.
[45] Mattila-Sandholm T, Wirtanen G. Biofilm formation in the industry: a review. Food Rev Int 1992;8:573–603.
[46] Jhajharia K, Parolia A, Shetty KV, Mehta LK. Biofilm in endodontics: a review. J Int Soc Prevent Commun Dent 2015;5:1.
[47] Horn H, Lackner S. Modeling of biofilm systems: a review. Productive Biofilms. Springer; 2014. p. 53–76.
[48] Campoccia D, Montanaro L, Arciola CR. A review of the biomaterials technologies for infection-resistant surfaces. Biomaterials 2013;34:8533–54.
[49] Graham MV, Mosier AP, Kiehl TR, Kaloyeros AE, Cady NC. Development of antifouling surfaces to reduce bacterial attachment. Soft Matter 2013;9:6235–44.
[50] Merritt PM, Danhorn T, Fuqua C. Motility and chemotaxis in agrobacterium tumefaciens surface attachment and biofilm formation. J Bacteriol 2007;189: 8005–14.
[51] Teodósio JS, Silva FC, Moreira JM, Simões M, Melo LF, Alves MA, et al. Flow cells as quasi-ideal systems for biofouling simulation of industrial piping systems. Biofouling 2013;29:953–66.
[52] Stoodley P, Dodds I, De Beer D, Scott HL, Boyle J. Flowing biofilms as a transport mechanism for biomass through porous media under laminar and turbulent conditions in a laboratory reactor system. Biofouling 2005;21:161–8.
[53] Tsai Y-P. Impact of flow velocity on the dynamic behaviour of biofilm bacteria. Biofouling 2005;21:267–77.
[54] Simoes M, Pereira MO, Sillankorva S, Azeredo J, Vieira MJ. The effect of hydrodynamic conditions on the phenotype of pseudomonas fluorescens biofilms. Biofouling 2007;23:249–58.
[55] Stoodley P, Dodds I, Boyle JD, Lappin-Scott H. Influence of hydrodynamics and nutrients on biofilm structure. J Appl Microbiol 1998;85:19S–28S.
[56] Besemer K, Singer G, Limberger R, Chlup A-K, Hochedlinger G, Hödl I, et al. Biophysical controls on community succession in stream biofilms. Appl Environ Microbiol 2007;73:4966–74.
[57] Pereira MO, Kuehn M, Wuertz S, Neu T, Melo LF. Effect of flow regime on the architecture of a pseudomonas fluorescens biofilm. Biotechnol Bioeng 2002;78:164–71.
[58] Santos R, Callow ME, Bott T. The structure of pseudomonas fluorescens biofilms in contact with flowing systems. Biofouling 1991;4:319–36.
[59] Carniello V, Peterson BW, van der Mei HC, Busscher HJ. Physico-chemistry from initial bacterial adhesion to surface-programmed biofilm growth. Adv Colloid Interface Sci 2018;261:1–14.
[60] Stoodley P, Lewandowski Z, Boyle JD, Lappin-Scott HM. The formation of migratory ripples in a mixed species bacterial biofilm growing in turbulent flow. Environ Microbiol 1999;1:447–55.
[61] Picioreanu C, Vrouwenvelder J, Van Loosdrecht M. Three-dimensional modeling of biofouling and fluid dynamics in feed spacer channels of membrane devices. J Membr Sci 2009;345:340–54.
[62] Boyle J, Lappin-Scott H. Quantification of the effect of flowrate on the rates of arrival and attachment to glass of pseudomonas aeruginosa. Biofouling 2006;22: 117–23.
[63] Zhang T, Cogan N, Wang Q. Phase-field models for biofilms ii. 2-d numerical simulations of biofilm-flow interaction. Commun Comput Phys 2008;4:72–101.
[64] Parvinzadeh Gashti M, Bellavance J, Kroukamp O, Wolfaardt G, Taghavi SM, Greener J. Live-streaming: time-lapse video evidence of novel streamer formation mechanism and varying viscosity. Biomicrofluidics 2015;9:041101.
[65] Thomen P, Robert J, Monmeyran A, Bitbol A-F, Douarche C, Henry N. Bacterial biofilm under flow: first a physical struggle to stay, then a matter of breathing. PLoS One 2017;12.
[66] Manz B, Volke F, Goll D, Horn H. Measuring local flow velocities and biofilm structure in biofilm systems with magnetic resonance imaging (mri). Biotechnol Bioeng 2003;84:424–32.
[67] Stoodley P, Boyle JD, DeBeer D, Lappin-Scott HM. Evolving perspectives of biofilm structure. Biofouling 1999;14:75–90.
[68] Purevdorj B, Costerton JW, Stoodley P. Influence of hydrodynamics and cell signaling on the structure and behavior of pseudomonas aeruginosa biofilms. Appl Environ Microbiol 2002;68:4457–64.
[69] Dunsmore B, Jacobsen A, Hall-Stoodley L, Bass C, Lappin-Scott H, Stoodley P. The influence of fluid shear on the structure and material properties of sulphate-reducing bacterial biofilms. J Ind Microbiol Biotechnol 2002;29:347–53.
[70] Stoodley P, Lewandowski Z, Boyle JD, Lappin-Scott HM. Structural deformation of bacterial biofilms caused by short-term fluctuations in fluid shear: An in situ investigation of biofilm rheology. Biotechnol Bioeng 1999;65:83–92.
[71] Rusconi R, Lecuyer S, Autrusson N, Guglielmini L, Stone HA. Secondary flow as a mechanism for the formation of biofilm streamers. Biophys J 2011;100:1392–9.
[72] Biswas I, Ghosh R, Sadrzadeh M, Kumar A. Near wall void growth leads to disintegration of colloidal bacterial streamer. J Colloid Interface Sci 2018;522:249–55.
[73] Taherzadeh D, Picioreanu C, Küttler U, Simone A, Wall WA, Horn H. Computational study of the drag and oscillatory movement of biofilm streamers in fast flows. Biotechnol Bioeng 2010;105:600–10.
[74] Guimerà X, Dorado AD, Bonsfills A, Gabriel G, Gabriel D, Gamisans X. Dynamic characterization of external and internal mass transport in heterotrophic biofilms from microsensors measurements. Water Res 2016;102:551–60.
[75] Garrett TR, Bhakoo M, Zhang Z. Bacterial adhesion and biofilms on surfaces. Prog Nat Sci 2008;18:1049–56.
[76] Moreira J, Simões M, Melo L, Mergulhão F. The combined effects of shear stress and mass transfer on the balance between biofilm and suspended cell dynamics. Desalin Water Treat 2015;53:3348–54.
[77] Radu AI, Vrouwenvelder JS, Van Loosdrecht M, Picioreanu C. Effect of flow velocity, substrate concentration and hydraulic cleaning on biofouling of reverse osmosis feed channels. Chem Eng J 2012;188:30–9.
[78] Oder M, Arlič M, Bohinc K, Fink R. Escherichia coli biofilm formation and dispersion under hydrodynamic conditions on metal surfaces. Int J Environ Health Res 2018; 28:55–63.
[79] Ohashi A, Koyama T, Syutsubo K, Harada H. A novel method for evaluation of biofilm tensile strength resisting erosion. Water Sci Technol 1999;39:261–8.
[80] Van Loosdrecht M, Eikelboom D, Gjaltema A, Mulder A, Tijhuis L, Heijnen J. Biofilm structures. Water Sci Technol 1995;32:35.
[81] Korber DR, Lawrence JR, Caldwell DE. Effect of motility on surface colonization and reproductive success of pseudomonas fluorescens in dual-dilution continuous culture and batch culture systems. Appl Environ Microbiol 1994;60:1421–9.
[82] Costerton JW. Overview of microbial biofilms. J Ind Microbiol 1995;15:137–40.
[83] Costerton JW, Lewandowski Z, Caldwell DE, Korber DR, Lappin-Scott HM. Microbial biofilms. Annu Rev Microbiol 1995;49:711–45.
[84] Wilking JN, Zaburdaev V, De Volder M, Losick R, Brenner MP, Weitz DA. Liquid transport facilitated by channels in bacillus subtilis biofilms. Proc Natl Acad Sci 2013;110:848–52.
[85] Robinson RW, Akin DE, Nordstedt RA, Thomas MV, Aldrich HC. Light and electron microscopic examinations of methane-producing biofilms from anaerobic fixed-bed reactors. Appl Environ Microbiol 1984;48:127–36.
[86] De Beer D, Stoodley P, Roe F, Lewandowski Z. Effects of biofilm structures on oxygen distribution and mass transport. Biotechnol Bioeng 1994;43:1131–8.
[87] Donlan RM, Costerton JW. Biofilms: survival mechanisms of clinically relevant microorganisms. Clin Microbiol Rev 2002;15:167–93.
[88] Li J, Busscher HJ, Norde W, Sjollema J. Analysis of the contribution of sedimentation to bacterial mass transport in a parallel plate flow chamber. Colloids Surf B Biointerfaces 2011;84:76–81.
[89] Busscher HJ, van der Mei HC. Microbial adhesion in flow displacement systems. Clin Microbiol Rev 2006;19:127–41.
[90] Stewart PS. Mini-review: convection around biofilms. Biofouling 2012;28:187–98.
[91] Teodósio J, Simões M, Melo L, Mergulhão F. Flow cell hydrodynamics and their effects on e. coli biofilm formation under different nutrient conditions and turbulent flow. Biofouling 2011;27:1–11.
[92] Margalit E, Leshansky A, Freger V. Modeling and analysis of hydrodynamic and physico-chemical effects in bacterial deposition on surfaces. Biofouling 2013;29: 977–89.
[93] Mukherjee PK, Chand DV, Chandra J, Anderson JM, Ghannoum MA. Shear stress modulates the thickness and architecture of candida albicans biofilms in a phase-dependent manner. Mycoses 2009;52:440–6.
[94] Blenkinsopp S, Costerton J. Understanding bacterial biofilms. Trends Biotechnol 1991;9:138–43.
[95] Berne C, Ellison CK, Ducret A, Brun YV. Bacterial adhesion at the single-cell level. Nat Rev Microbiol 2018;16:616–27.
[96] Conrad JC. Physics of bacterial near-surface motility using flagella and type iv pili: implications for biofilm formation. Res Microbiol 2012;163:619–29.
[97] Lindsay D, Von Holy A. Bacterial biofilms within the clinical setting: what healthcare professionals should know. J Hosp Infect 2006;64:313–25.
[98] Busscher H, Van der Mei H. Physico-chemical interactions in initial microbial adhesion and relevance for biofilm formation. Adv Dent Res 1997;11:24–32.
[99] Busscher HJ, Weerkamp AH. Specific and non-specific interactions in bacterial adhesion to solid substrata. FEMS Microbiol Rev 1987;3:165–73.
[100] Vigeant MA-S, Ford RM, Wagner M, Tamm LK. Reversible and irreversible adhesion of motile escherichia coli cells analyzed by total internal reflection aqueous fluorescence microscopy. Appl Environ Microbiol 2002;68:2794–801.
[101] Kimkes TE, Heinemann M. How bacteria recognise and respond to surface contact. FEMS Microbiol Rev 2020;44:106–22.
[102] Goldman AJ, Cox RG, Brenner H. Slow viscous motion of a sphere parallel to a plane wall—i motion through a quiescent fluid. Chem Eng Sci 1967;22:637–51.
[103] de Haan HW. Modeling and simulating the dynamics of type iv pili extension of pseudomonas aeruginosa. Biophys J 2016;111:2263–73.
[104] Wong WY, McInnes C, Sykes BD, Paranchych W, Irvin RT, Hodges RS. Structure-function analysis of the adherence-binding domain on the pilin of pseudomonas aeruginosa strains pak and kb7. Biochemistry 1995;34:12963–72.
[105] Harvey H, Habash M, Aidoo F, Burrows LL. Single-residue changes in the c-terminal disulfide-bonded loop of the pseudomonas aeruginosa type iv pilin influence pilus assembly and twitching motility. J Bacteriol 2009;191:6513–24.
[106] Shen Y, Siryaporn A, Lecuyer S, Gitai Z, Stone HA. Flow directs surface-attached bacteria to twitch upstream. Biophys J 2012;103:146–51.
[107] Ghosh R, Kumar A, Vaziri A. Type-iv pilus deformation can explain retraction behavior. PLoS One 2014;9:e114613.
[108] Jin F, Conrad JC, Gibiansky ML, Wong GC. Bacteria use type-iv pili to slingshot on surfaces. Proc Natl Acad Sci 2011;108:12617–22.

[109] Nejadnik MR, Van Der Mei HC, Busscher HJ, Norde W. Determination of the shear force at the balance between bacterial attachment and detachment in weak-adherence systems, using a flow displacement chamber. Appl Environ Microbiol 2008;74:916–9.
[110] Saur T, Morin E, Habouzit F, Bernet N, Escudié R. Impact of wall shear stress on initial bacterial adhesion in rotating annular reactor. PLoS One 2017;12.
[111] Wen J, Gu T, Nesic S, et al. Investigation of the effects of fluid flow on srb biofilm. NACE International corrosion conference series, corrosion/2007 Paper, 07516; 2007.
[112] Linton C, Sherriff A, Millar M. Use of a modified Robbins device to directly compare the adhesion of staphylococcus epidermidis rp62a to surfaces. J Appl Microbiol 1999;86:194–202.
[113] Rieu A, Briandet R, Habimana O, Garmyn D, Guzzo J, Piveteau P. Listeria monocytogenes egd-e biofilms: no mushrooms but a network of knitted chains. Appl Environ Microbiol 2008;74:4491–7.
[114] Agladze K, Jackson D, Romeo T. Periodicity of cell attachment patterns during escherichia coli biofilm development. J Bacteriol 2003;185:5632–8.
[115] Stewart PS, Franklin MJ. Physiological heterogeneity in biofilms. Nat Rev Microbiol 2008;6:199–210.
[116] Tolker-Nielsen T, Molin S. Spatial organization of microbial biofilm communities. Microb Ecol 2000;40:75–84.
[117] Oliveira NM, Foster KR, Durham WM. Single-cell twitching chemotaxis in developing biofilms. Proc Natl Acad Sci 2016;113:6532–7.
[118] Greiner L, Edwards J, Shao J, Rabinak C, Entz D, Apicella M. Biofilm formation by neisseria gonorrhoeae. Infect Immun 2005;73:1964–70.
[119] Leon Ohl A, Horn H, Hempel D. Behaviour of biofilm systems under varying hydrodynamic conditions. Water Sci Technol 2004;49:345–51.
[120] Brugnoni LI, Cubitto MA, Lozano JE. Candida krusei development on turbulent flow regimes: biofilm formation and efficiency of cleaning and disinfection program. J Food Eng 2012;111:546–52.
[121] Vieira MJ, Melo LF, Pinheiro MM. Biofilm formation: hydrodynamic effects on internal diffusion and structure. Biofouling 1993;7:67–80.
[122] Douterelo I, Sharpe R, Boxall J. Influence of hydraulic regimes on bacterial community structure and composition in an experimental drinking water distribution system. Water Res 2013;47:503–16.
[123] Liu Y, Tay J-H. Metabolic response of biofilm to shear stress in fixed-film culture. J Appl Microbiol 2001;90:337–42.
[124] Jones A-AD, Buie CR. Shear stress mediates metabolism and growth in electroactive biofilms. BioRxiv 2018;391029.
[125] Simões M, Simões LC, Machado I, Pereira MO, Vieira MJ. Control of flow-generated biofilms with surfactants: evidence of resistance and recovery. Food Bioprod Process 2006;84:338–45.
[126] de Beer D, Stoodley P, Lewandowski Z. Liquid flow in heterogeneous biofilms. Biotechnol Bioeng 1994;44:636–41.
[127] de Beer D, Stoodley P. Relation between the structure of an aerobic biofilm and transport phenomena. Water Sci Technol 1995;32:11–8.
[128] Dunne WM. Bacterial adhesion: seen any good biofilms lately? Clin Microbiol Rev 2002;15:155–66.
[129] O'Toole G, Kaplan HB, Kolter R. Biofilm formation as microbial development. Annu Rev Microbiol 2000;54:49–79.
[130] Pearce P, Song B, Skinner DJ, Mok R, Hartmann R, Singh PK, et al. Flow-induced symmetry breaking in growing bacterial biofilms. Phys Rev Lett 2019;123:258101.
[131] Hassanpourfard M, Ghosh R, Thundat T, Kumar A. Dynamics of bacterial streamers induced clogging in microfluidic devices. Lab Chip 2016;16:4091–6.
[132] Stoodley P, DeBeer D, Lewandowski Z. Liquid flow in biofilm systems. Appl Environ Microbiol 1994;60:2711–6.
[133] Lawrence J, Korber D, Hoyle B, Costerton JW, Caldwell D. Optical sectioning of microbial biofilms. J Bacteriol 1991;173:6558–67.
[134] Davey ME, O'toole GA. Microbial biofilms: from ecology to molecular genetics. Microbiol Mol Biol Rev 2000;64:847–67.
[135] Reichert P, Wanner O. Movement of solids in biofilms: significance of liquid phase transport. Water Sci Technol 1997;36:321–8.
[136] Stoodley P, Sauer K, Davies DG, Costerton JW. Biofilms as complex differentiated communities. Annu Rev Microbiol 2002;56:187–209.
[137] Massol-Deyá AA, Whallon J, Hickey RF, Tiedje JM. Channel structures in aerobic biofilms of fixed-film reactors treating contaminated groundwater. Appl Environ Microbiol 1995;61:769–77.
[138] Battin TJ, Kaplan LA, Newbold JD, Hansen CM. Contributions of microbial biofilms to ecosystem processes in stream mesocosms. Nature 2003;426:439–42.
[139] Kühl M, Jørgensen BB. Microsensor measurements of sulfate reduction and sulfide oxidation in compact microbial communities of aerobic biofilms. Appl Environ Microbiol 1992;58:1164–74.
[140] Folsom JP, Richards L, Pitts B, Roe F, Ehrlich GD, Parker A, et al. Physiology of pseudomonas aeruginosa in biofilms as revealed by transcriptome analysis. BMC Microbiol 2010;10:294.
[141] Kühl M, Rickelt LF, Thar R. Combined imaging of bacteria and oxygen in biofilms. Appl Environ Microbiol 2007;73:6289–95.
[142] Seminara A, Angelini TE, Wilking JN, Vlamakis H, Ebrahim S, Kolter R, et al. Osmotic spreading of bacillus subtilis biofilms driven by an extracellular matrix. Proc Natl Acad Sci 2012;109:1116–21.
[143] Costerton JW, Lewandowski Z, DeBeer D, Caldwell D, Korber D, James G. Biofilms, the customized microniche. J Bacteriol 1994;176:2137.
[144] Picioreanu C, Van Loosdrecht MC, Heijnen JJ. Mathematical modeling of biofilm structure with a hybrid differential-discrete cellular automaton approach. Biotechnol Bioeng 1998;58:101–16.
[145] Alfred B. Cunningham, John E. Lennox, and Rockford J. Ross, 2010. Biofilms: the hypertextbook. https://wwwcsmontanaedu/webworks/projects/stevesbook/contents/chapters/chapter010/section003/blue/page001html [Visited: 2020-06-05].
[146] Ploux L, Beckendorff S, Nardin M, Neunlist S. Quantitative and morphological analysis of biofilm formation on self-assembled monolayers. Colloids Surf B Biointerfaces 2007;57:174–81.
[147] Crusz SA, Popat R, Rybtke MT, Cámara M, Givskov M, Tolker-Nielsen T, et al. Bursting the bubble on bacterial biofilms: a flow cell methodology. Biofouling 2012;28:835–42.
[148] Fabbri S, Li J, Howlin RP, Rmaile A, Gottenbos B, De Jager M, et al. Fluid-driven interfacial instabilities and turbulence in bacterial biofilms. Environ Microbiol 2017;19:4417–31.
[149] Miles JW. On the generation of surface waves by shear flows part 3. Kelvin-helmholtz instability. J Fluid Mech 1959;6:583–98.
[150] Funada T, Joseph D. Viscous potential flow analysis of kelvin-helmholtz instability in a channel. J Fluid Mech 2001;445:263–83.
[151] Andrewartha J, Sargison J, Perkins K. The effect of gomphonema and filamentous algae streamers on hydroelectric canal capacity and turbulent boundary layer structure; 2007.
[152] Schultz MP. Turbulent boundary layers on surfaces covered with filamentous algae. J Fluids Eng 2000;122:357–63.
[153] Picologlou BF, Zelver N, Characklis WG. Biofilm growth and hydraulic performance. J Hydraul Div 1980;106:733–46.
[154] McCoy W, Bryers J, Robbins J, Costerton J. Observations of fouling biofilm formation. Can J Microbiol 1981;27:910–7.
[155] Andrewartha J, Sargison J, et al. Turbulence and mean-velocity structure of flows over filamentous biofilms. In Proceedings of the 34th world congress of the International Association for Hydro-Environment Research and Engineering: 33rd hydrology and water resources symposium and 10th conference on hydraulics in water engineering, p. 2225. Engineers Australia; 2011.
[156] Liu N, Skauge T, Landa-Marbán D, Hovland B, Thorbjørnsen B, Radu FA, et al. Microfluidic study of effects of flow velocity and nutrient concentration on biofilm accumulation and adhesive strength in the flowing and no-flowing microchannels. J Ind Microbiol Biotechnol 2019;46:855–68.
[157] Valiei A, Kumar A, Mukherjee PP, Liu Y, Thundat T. A web of streamers: biofilm formation in a porous microfluidic device. Lab Chip 2012;12:5133–7.
[158] Hassanpourfard M, Nikakhtari Z, Ghosh R, Das S, Thundat T, Liu Y, et al. Bacterial floc mediated rapid streamer formation in creeping flows. Sci Rep 2015;5:13070.
[159] Debnath N, Kumar A, Thundat T, Sadrzadeh M. Investigating fouling at the pore-scale using a microfluidic membrane mimic filtration system. Sci Rep 2019;9:1–10.
[160] Biswas I, Sadrzadeh M, Kumar A. Impact of bacterial streamers on biofouling of microfluidic filtration systems. Biomicrofluidics 2018;12:044116.
[161] Stoodley P, Boyle J, Cunningham AB, Dodds I, Lappin-Scott H, Lewandowski Z. Biofilm structure and influence on biofouling under laminar and turbulent flows. , 242Special Publication-Royal Society of Chemistry; 1999; 13–24.
[162] Stoodley P, Lewandowski Z, Boyle JD, Lappin-Scott HM. Oscillation characteristics of biofilm streamers in turbulent flowing water as related to drag and pressure drop. Biotechnol Bioeng 1998;57:536–44.
[163] Stoodley P, Boyle JD, Lappin-Scott HM. Influence of flow on the structure of bacterial biofilms; 2000.
[164] Drescher K, Shen Y, Bassler BL, Stone HA. Biofilm streamers cause catastrophic disruption of flow with consequences for environmental and medical systems. Proc Natl Acad Sci 2013;110:4345–50.
[165] Biswas I, Ghosh R, Sadrzadeh M, Kumar A. Nonlinear deformation and localized failure of bacterial streamers in creeping flows. Sci Rep 2016;6:32204.
[166] Vrouwenvelder J, Von Der Schulenburg DG, Kruithof J, Johns M, Van Loosdrecht M. Biofouling of spiral-wound nanofiltration and reverse osmosis membranes: a feed spacer problem. Water Res 2009;43:583–94.
[167] Marty A, Roques C, Causserand C, Bacchin P. Formation of bacterial streamers during filtration in microfluidic systems. Biofouling 2012;28:551–62.
[168] Scheidweiler D, Peter H, Pramateftaki P, De Anna P, Battin TJ. Unraveling the biophysical underpinnings to the success of multispecies biofilms in porous environments. ISME J 2019;13:1700–10.
[169] Towler BW, Rupp CJ, Cunningham AB, Stoodley P. Viscoelastic properties of a mixed culture biofilm from rheometer creep analysis. Biofouling 2003;19:279–85.
[170] Klapper I, Rupp CJ, Cargo R, Purvedorj B, Stoodley P. Viscoelastic fluid description of bacterial biofilm material properties. Biotechnol Bioeng 2002;80:289–96.
[171] Yazdi S, Ardekani AM. Bacterial aggregation and biofilm formation in a vortical flow. Biomicrofluidics 2012;6:044114.
[172] Horemans B, Hofkens J, Smolders E, Springael D. Biofilm formation of a bacterial consortium on linuron at micropollutant concentrations in continuous flow chambers and the impact of dissolved organic matter. FEMS Microbiol Ecol 2014;88:184–94.
[173] Wang X, Hao M, Du X, Wang G, Matsushita J-I. The mechanical analysis of the biofilm streamer nucleation and geometry characterization in microfluidic channels. Comput Math Methods Med 2016;2016.
[174] Besemer K, Hödl I, Singer G, Battin TJ. Architectural differentiation reflects bacterial community structure in stream biofilms. ISME J 2009;3:1318–24.
[175] Taherzadeh D. Mechanics and substrate transport of moving biofilm structures. Ph. D. thesis. Technische Universität München; 2011.
[176] Rusconi R, Lecuyer S, Guglielmini L, Stone HA. Laminar flow around corners triggers the formation of biofilm streamers. J R Soc Interface 2010;7:1293–9.
[177] Debnath N, Hassanpourfard M, Ghosh R, Thundat T, Sadrzadeh M, Kumar A. Abiotic streamers in a microfluidic system. Soft Matter 2017;13:8698–705.

[178] Debnath N, Sadrzadeh M. Microfluidic mimic for colloid membrane filtration: a review. J Indian Inst Sci 2018;98:137–57.
[179] Valiei A. Biofilm streamer formation in a porous microfluidic device; 2013.
[180] Picioreanu C, van Loosdrecht MC, Heijnen JJ. A theoretical study on the effect of surface roughness on mass transport and transformation in biofilms. Biotechnol Bioeng 2000;68:355–69.
[181] Picard C, Logette S, Schrotter J-C, Aimar P, Remigy J-C. Mass transfer in a membrane aerated biofilm. Water Res 2012;46:4761–9.
[182] Kugaprasatham S, Nagaoka H, Ohgaki S. Effect of turbulence on nitrifying biofilms at non-limiting substrate conditions. Water Res 1992;26:1629–38.
[183] Cowle MW, Webster G, Babatunde AO, Bockelmann-Evans BN, Weightman AJ. Impact of flow hydrodynamics and pipe material properties on biofilm development within drinking water systems. Environ Technol 2019:1–13.
[184] Finlay JA, Schultz MP, Cone G, Callow ME, Callow JA. A novel biofilm channel for evaluating the adhesion of diatoms to non-biocidal coatings. Biofouling 2013;29:401–11.
[185] Tsagkari E, Sloan W. Turbulence accelerates the growth of drinking water biofilms. Bioprocess Biosyst Eng 2018;41:757–70.
[186] Santos R, Bott T, Callow M. Coated surfaces in relation to biofilm formation. Biofilms—science and technology. Springer; 1992. p. 105–10.
[187] Perni S, Jordan SJ, Andrew PW, Shama G. Biofilm development by listeria innocua in turbulent flow regimes. Food Control 2006;17:875–83.
[188] Cowle MW, Babatunde AO, Bockelmann-Evans BN. The frictional resistance induced by bacterial based biofouling in drainage pipelines. J Hydraul Res 2017;55:269–83.
[189] Andrewartha JM. The effect of freshwater biofilms on turbulent boundary layers and the implications for hydropower canals. Ph.D. thesis. University of Tasmania; 2010.
[190] Celmer D, Oleszkiewicz J, Cicek N. Impact of shear force on the biofilm structure and performance of a membrane biofilm reactor for tertiary hydrogen-driven denitrification of municipal wastewater. Water Res 2008;42:3057–65.
[191] Murphy EA, Barros JM, Schultz MP, Flack KA, Steppe CN, Reidenbach MA. Roughness effects of diatomaceous slime fouling on turbulent boundary layer hydrodynamics. Biofouling 2018;34:976–88.
[192] Schultz M, Swain G. The effect of biofilms on turbulent boundary layers; 1999.
[193] Schultz M, Walker J, Steppe C, Flack K. Impact of diatomaceous biofilms on the frictional drag of fouling-release coatings. Biofouling 2015;31:759–73.
[194] Hartenberger JD, Callison EG, Gose JW, Perlin M, Ceccio SL. Drag production mechanisms of filamentous biofilms. Biofouling 2020;36:736–52.
[195] Magin CM, Long CJ, Cooper SP, Ista LK, López GP, Brennan AB. Engineered antifouling microtopographies: the role of Reynolds number in a model that predicts attachment of zoospores of ulva and cells of cobetia marina. Biofouling 2010;26:719–27.
[196] Bryers J, Characklis W. Early fouling biofilm formation in a turbulent flow system: overall kinetics. Water Res 1981;15:483–91.
[197] Gjaltema A, Arts P, Van Loosdrecht M, Kuenen J, Heijnen J. Heterogeneity of biofilms in rotating annular reactors: occurrence, structure, and consequences. Biotechnol Bioeng 1994;44:194–204.
[198] Neu TR, Lawrence JR. Development and structure of microbial biofilms in river water studied by confocal laser scanning microscopy. FEMS Microbiol Ecol 1997;24:11–25.
[199] Lawrence J, Swerhone G, Neu T. A simple rotating annular reactor for replicated biofilm studies. J Microbiol Methods 2000;42:215–24.
[200] Horn H, Reiff H, Morgenroth E. Simulation of growth and detachment in biofilm systems under defined hydrodynamic conditions. Biotechnol Bioeng 2003;81:607–17.
[201] Wang H, Masters S, Edwards MA, Falkinham III JO, Pruden A. Effect of disinfectant, water age, and pipe materials on bacterial and eukaryotic community structure in drinking water biofilm. Environ Sci Technol 2014;48:1426–35.
[202] Rumbaugh KP, Sauer K. Biofilm dispersion. Nat Rev Microbiol 2020:1–16.
[203] Ebrahimi S, Picioreanu C, Xavier J, Kleerebezem R, Kreutzer M, Kapteijn F, et al. Biofilm growth pattern in honeycomb monolith packings: effect of shear rate and substrate transport limitations. Catal Today 2005;105:448–54.
[204] Gibson H, Taylor J, Hall K, Holah J. Effectiveness of cleaning techniques used in the food industry in terms of the removal of bacterial biofilms. J Appl Microbiol 1999;87:41–8.
[205] Meyer B. Approaches to prevention, removal and killing of biofilms. Int Biodeter Biodegr 2003;51:249–53.
[206] Sohn SY, Alfa MJ, Lai R, Tabani Y, Labib ME. Turbulent fluid flow is a novel closed-system sample extraction method for flexible endoscope channels of various inner diameters. J Microbiol Methods 2020;168:105782.
[207] Blanchard AP, Bird MR, Wright SJL. Peroxygen disinfection of pseudomonas aeruginosa biofilms on stainless steel discs. Biofouling 1998;13:233–53.
[208] Kaplan Já. Biofilm dispersal: mechanisms, clinical implications, and potential therapeutic uses. J Dent Res 2010;89:205–18.
[209] Telgmann U, Horn H, Morgenroth E. Influence of growth history on sloughing and erosion from biofilms. Water Res 2004;38:3671–84.
[210] Picioreanu C, Van Loosdrecht MC, Heijnen JJ. Two-dimensional model of biofilm detachment caused by internal stress from liquid flow. Biotechnol Bioeng 2001;72:205–18.
[211] Fink R, Oder M, Rangus D, Raspor P, Bohinc K. Microbial adhesion capacity. Influence of shear and temperature stress. Int J Environ Health Res 2015;25:656–69.
[212] Zarabadi MP, Paquet-Mercier F, Charette SJ, Greener J. Hydrodynamic effects on biofilms at the biointerface using a microfluidic electrochemical cell: case study of pseudomonas sp. Langmuir 2017;33:2041–9.
[213] Renner LD, Weibel DB. Physicochemical regulation of biofilm formation. MRS Bull 2011;36:347–55.
[214] Vasudevan R. Biofilms: microbial cities of scientific significance. J Microbiol Exp 2014;1:00014.
[215] Narayana S, Srihari S. A review on surface modifications and coatings on implants to prevent biofilm. Regen Eng Transl Med 2019;6:330–46.
[216] Salta M, Wharton JA, Blache Y, Stokes KR, Briand J-F. Marine biofilms on artificial surfaces: structure and dynamics. Environ Microbiol 2013;15:2879–93.
[217] Pollard A, House H. An unusual deposit in a hydraulic tunnel. J Power Div 1959;85:163–72.
[218] Manuel CM, Nunes OC, Melo L. Dynamics of drinking water biofilm in flow/non-flow conditions. Water Res 2007;41:551–62.
[219] Proctor CR, Gächter M, Kötzsch S, Rölli F, Sigrist R, Walser J-C, et al. Biofilms in shower hoses–choice of pipe material influences bacterial growth and communities. Environ Sci Water Res Technol 2016;2:670–82.
[220] Gulati P, Ghosh M. Biofilm forming ability of sphingomonas paucimobilis isolated from community drinking water systems on plumbing materials used in water distribution. J Water Health 2017;15:942–54.
[221] Papciak D, Tchórzewska-Cieślak B, Domoń A, Wojtuś A, Żywiec J, Konkol J. The impact of the quality of tap water and the properties of installation materials on the formation of biofilms. Water 2019;11:1903.
[222] Chen M, Zhang Z, Bott T. Effects of operating conditions on the adhesive strength of pseudomonas fluorescens biofilms in tubes. Colloids Surf B Biointerfaces 2005;43:61–71.
[223] Tian, Y.-M., Liu, Y.-W. & Liu, H.-N., 2010 c. In 2010 4th international conference on bioinformatics and biomedical engineering, pp. 1–4. IEEE.
[224] Zhang C, Li C, Zheng X, Zhao J, He G, Zhang T. Effect of pipe materials on chlorine decay, trihalomethanes formation, and bacterial communities in pilot-scale water distribution systems. Int J Environ Sci Technol 2017;14:85–94.
[225] Rogers J, Dowsett A, Dennis P, Lee J, Keevil C. Influence of plumbing materials on biofilm formation and growth of legionella pneumophila in potable water systems. Appl Environ Microbiol 1994;60:1842–51.
[226] DeFlaun M, Oppenheimer S, Streger S, Condee C, Fletcher M. Alterations in adhesion, transport, and membrane characteristics in an adhesion-deficient pseudomonad. Appl Environ Microbiol 1999;65:759–65.
[227] Davies DG, Geesey GG. Regulation of the alginate biosynthesis gene algc in pseudomonas aeruginosa during biofilm development in continuous culture. Appl Environ Microbiol 1995;61:860–7.
[228] Barkarmo S, Longhorn D, Leer K, Johansson CB, Stenport V, Franco-Tabares S, et al. Biofilm formation on polyetheretherketone and titanium surfaces. Clin Exp Dental Res 2019;5:427–37.
[229] Muthukrishnan T, Al Khaburi M, Abed RM. Fouling microbial communities on plastics compared with wood and steel: are they substrate-or location-specific? Microb Ecol 2019;78:361–74.
[230] Vague M, Chan G, Roberts C, Swartz NA, Mellies JL. Pseudomonas isolates degrade and form biofilms on polyethylene terephthalate (pet) plastic. BioRxiv 2019: 647321.
[231] Rogers KL, Carreres-Calabuig JA, Gorokhova E, Posth NR. Micro-by-micro interactions: how microorganisms influence the fate of marine microplastics. Limnol Oceanogr Lett 2020;5:18–36.
[232] Assanta MA, Roy D, Montpetit D. Adhesion of aeromonas hydrophila to water distribution system pipes after different contact times. J Food Prot 1998;61:1321–9.
[233] Bezanson G, Burbridge S, Haldane D, Marrie T. In situ colonization of polyvinyl chloride, brass, and copper by legionella pneumophila. Can J Microbiol 1992;38:328–30.
[234] Schofield GM, Locci R. Colonization of components of a model hot water system by legionella pneumophila. J Appl Bacteriol 1985;58:151–62.
[235] Jonas RB. Acute copper and cupric ion toxicity in an estuarine microbial community. Appl Environ Microbiol 1989;55:43–9.
[236] Roberts JA. Inhibition and enhancement of microbial surface colonization: the role of silicate composition. Chem Geol 2004;212:313–27.
[237] Mafu AA, Roy D, Goulet J, Magny P. Attachment of listeria monocytogenes to stainless steel, glass, polypropylene, and rubber surfaces after short contact times. J Food Prot 1990;53:742–6.
[238] Lindner E. A low surface free energy approach in the control of marine biofouling. Biofouling 1992;6:193–205.
[239] Zhao Q, Liu C, Liu Y, Wang S. Bacterial and protein adhesion on ni-p-ptfe coated surfaces; 2007.
[240] Dexter S, Sullivan J, Williams J, Watson S. Influence of substrate wettability on the attachment of marine bacteria to various surfaces. Appl Environ Microbiol 1975;30:298–308.
[241] Akesso L, Navabpour P, Teer D, Pettitt ME, Callow ME, Liu C, et al. Deposition parameters to improve the fouling-release properties of thin siloxane coatings prepared by pacvd. Appl Surf Sci 2009;255:6508–14.
[242] Navabpour P, Teer D, Su X, Liu C, Wang S, Zhao Q, et al. Optimisation of the properties of siloxane coatings as anti-biofouling coatings: comparison of pacvd and hybrid pacvd–pvd coatings. Surf Coat Technol 2010;204:3188–95.
[243] Tsibouklis J, Stone M, Thorpe AA, Graham P, Nevell TG, Ewen RJ. Inhibiting bacterial adhesion onto surfaces: the non-stick coating approach. Int J Adhes Adhes 2000;20:91–6.
[244] Milne A, Callow M. Non-biocidal antifouling processes. Polymers in a marine environment conference; 1985.
[245] Liu C, Zhao Q. Influence of surface-energy components of ni–p–tio2–ptfe nanocomposite coatings on bacterial adhesion. Langmuir 2011;27:9512–9.
[246] Katsikogianni M, Missirlis Y. Interactions of bacteria with specific biomaterial surface chemistries under flow conditions. Acta Biomater 2010;6:1107–18.

[247] Zhang X, Wang L, Levänen E. Superhydrophobic surfaces for the reduction of bacterial adhesion. RSC Adv 2013;3:12003–20.
[248] Zhao Q, Wang S, Müller-Steinhagen H. Tailored surface free energy of membrane diffusers to minimize microbial adhesion. Appl Surf Sci 2004;230:371–8.
[249] Baier R. Adsorption of micro-organisms to surface. NY: Wiley–Interscience Publishers; 1980; 59–104.
[250] Pereni C, Zhao Q, Liu Y, Abel E. Surface free energy effect on bacterial retention. Colloids Surf B Biointerfaces 2006;48:143–7.
[251] Hamza A, Pham V, Matsuura T, Santerre J. Development of membranes with low surface energy to reduce the fouling in ultrafiltration applications. J Membr Sci 1997;131:217–27.
[252] Baier R. Substrata influences on adhesion of microorganisms and their resultant new surface properties. Adsorption of microorganisms to surfaces. New York: John Wiley; 1980. p. 59–104.
[253] Fryer PJ, Robbins PT, Asteriadou I. Current knowledge in hygienic design: can we minimise fouling and speed cleaning? Advances in food process engineering research and applications. Springer; 2013. p. 209–27.
[254] Becker K. Detachment studies on microfouling in natural biofilms on substrata with different surface tensions. Int Biodeter Biodegr 1998;41:93–100.
[255] Callow ME, Fletcher RL. The influence of low surface energy materials on bioadhesion—a review. Int Biodeter Biodegr 1994;34:333–48.
[256] Bohinc K, Dražić G, Oder M, Jevšnik M, Nipič D, Godič-Torkar K, et al. Available surface dictates microbial adhesion capacity. Int J Adhes Adhes 2014;50:265–72.
[257] Li B, Logan BE. Bacterial adhesion to glass and metal-oxide surfaces. Colloids Surf B Biointerfaces 2004;36:81–90.
[258] Bhandari B, Howes T. Relating the stickiness property of foods undergoing drying and dried products to their surface energetics. Drying Technol 2005;23:781–97.
[259] Amanatides E, Mataras D, Katsikogianni M, Missirlis Y. Plasma surface treatment of polyethylene terephthalate films for bacterial repellence. Surf Coat Technol 2006; 200:6331–5.
[260] Katsikogianni MG, Syndrevelis CS, Amanatides EK, Mataras DS, Missirlis YF. Plasma treated and a-c: H coated pet performance in inhibiting bacterial adhesion. Plasma Processes Polym 2007;4:S1046–51.
[261] Fonseca A, Granja P, Nogueira J, Oliveira D, Barbosa M. Staphylococcus epidermidis rp62a adhesion to chemically modified cellulose derivatives. J Mater Sci Mater Med 2001;12:543–8.
[262] Gallardo-Moreno AM, Pacha-Olivenza MA, Saldaña L, Pérez-Giraldo C, Bruque JM, Vilaboa N, et al. In vitro biocompatibility and bacterial adhesion of physico-chemically modified ti6al4v surface by means of uv irradiation. Acta Biomater 2009;5:181–92.
[263] Van Oss CJ. Interfacial forces in aqueous media. CRC press; 2006.
[264] Smith JR, Leveneur J, Kennedy JV. Design of intelligent surfaces for energy intensive processing industry. MATEC web of conferences. EDP Sciences; 2018. p. 00001.
[265] Liu C, Zhao Q. The cq ratio of surface energy components influences adhesion and removal of fouling bacteria. Biofouling 2011;27:275–85.
[266] Ma M, Hill RM. Superhydrophobic surfaces. Curr Opin Colloid Interface Sci 2006;11: 193–202.
[267] Song F, Koo H, Ren D. Effects of material properties on bacterial adhesion and biofilm formation. J Dent Res 2015;94:1027–34.
[268] Selim MS, Hao Z, Mo P, Jiang Y, Tan G. Superhydrophobic self-cleaning surfaces in nature. Nanoarchitectonics 2020:26–37.
[269] Yan YY, Gao N, Barthlott W. Mimicking natural superhydrophobic surfaces and grasping the wetting process: a review on recent progress in preparing superhydrophobic surfaces. Adv Colloid Interface Sci 2011;169:80–105.
[270] Qu M, Zhao G, Cao X, Zhang J. Biomimetic fabrication of lotus-leaf-like structured polyaniline film with stable superhydrophobic and conductive properties. Langmuir 2008;24:4185–9.
[271] Eduok U, Szpunar J, Ebenso E. Superhydrophobic antibacterial polymer coatings. Superhydrophobic polymer coatings. Elsevier; 2019. p. 245–79.
[272] Bruzaud J, Tarrade J, Celia E, Darmanin T, De Givenchy ET, Guittard F, et al. The design of superhydrophobic stainless steel surfaces by controlling nanostructures: a key parameter to reduce the implantation of pathogenic bacteria. Mater Sci Eng C 2017;73:40–7.
[273] Xu L-C, Meyerhoff ME, Siedlecki CA. Blood coagulation response and bacterial adhesion to biomimetic polyurethane biomaterials prepared with surface texturing and nitric oxide release. Acta Biomater 2019;84:77–87.
[274] Cheng Y, Feng G, Moraru CI. Micro-and nanotopography sensitive bacterial attachment mechanisms: a review. Front Microbiol 2019;10.
[275] Schumacher JF, Carman ML, Estes TG, Feinberg AW, Wilson LH, Callow ME, et al. Engineered antifouling microtopographies–effect of feature size, geometry, and roughness on settlement of zoospores of the green alga ulva. Biofouling 2007;23: 55–62.
[276] Schumacher JF, Long CJ, Callow ME, Finlay JA, Callow JA, Brennan AB. Engineered nanoforce gradients for inhibition of settlement (attachment) of swimming algal spores. Langmuir 2008;24:4931–7.
[277] An R, Dong Y, Zhu J, Rao C. Adhesion and friction forces in biofouling attachments to nanotube-and peg-patterned tio2 surfaces. Colloids Surf B Biointerfaces 2017; 159:108–17.
[278] Díaz C, Cortizo MC, Schilardi PL, Saravia SGGD, Mele MAFLD. Influence of the nano-micro structure of the surface on bacterial adhesion. Mater Res 2007;10:11–4.
[279] Liduino VS, Cravo-Laureau C, Noel C, Carbon A, Duran R, Lutterbach MT, et al. Comparison of flow regimes on biocorrosion of steel pipe weldments: community composition and diversity of biofilms. Int Biodeter Biodegr 2019;143:104717.
[280] Kumar A, Karig D, Acharya R, Neethirajan S, Mukherjee PP, Retterer S, et al. Microscale confinement features can affect biofilm formation. Microfluid Nanofluid 2013;14:895–902.
[281] Bollen C. Lambrechts p andquiryen m. comparison of surface roughness of oral hard materials to the threshold surface roughness for bacterial plaque retention: a review of the literature. Dent Mater 1997;13:258–69.
[282] Arnold J, Bailey G. Surface finishes on stainless steel reduce bacterial attachment and early biofilm formation: scanning electron and atomic force microscopy study. Poult Sci 2000;79:1839–45.
[283] Medilanski E, Kaufmann K, Wick LY, Wanner O, Harms H. Influence of the surface topography of stainless steel on bacterial adhesion. Biofouling 2002;18:193–203.
[284] Boulangé-Petermann L, Rault J, Bellon-Fontaine M-N. Adhesion of streptococcus thermophilus to stainless steel with different surface topography and roughness. Biofouling 1997;11:201–16.
[285] Flint S, Brooks J, Bremer P. Properties of the stainless steel substrate, influencing the adhesion of thermo-resistant streptococci. J Food Eng 2000;43:235–42.
[286] Tide C, Harkin SR, Geesey GG, Bremer PJ, Scholz W. The influence of welding procedures on bacterial colonization of stainless steel weldments. J Food Eng 1999; 42:85–96.
[287] Vanhaecke E, Remon J, Moors M, Raes F, De Rudder D, Van Peteghem A. Kinetics of pseudomonas aeruginosa adhesion to 304 and 316-l stainless steel: role of cell surface hydrophobicity. Appl Environ Microbiol 1990;56:788–95.
[288] Dantas, L. C. D. M., Silva-Neto, J. P. D., Dantas, T. S., Naves, L. Z., das Neves, F. D. & da Mota, A. S., 2016 Bacterial adhesion and surface roughness for different clinical techniques for acrylic polymethyl methacrylate. Int J Dent 2016.
[289] Encinas N, Yang C-Y, Geyer F, Kaltbeitzel A, Baumli P, Reinholz J, et al. Submicrometer-sized roughness suppresses bacteria adhesion. ACS Appl Mater Interfaces 2020.
[290] Mitik-Dineva N, Wang J, Mocanasu RC, Stoddart PR, Crawford RJ, Ivanova EP. Impact of nano-topography on bacterial attachment. Biotechnol J 2008;3:536–44.
[291] Mitik-Dineva N, Wang J, Truong V, Stoddart P, Malherbe F, Crawford R, et al. Differences in colonisation of five marine bacteria on two types of glass surfaces. Biofouling 2009;25:621–31.
[292] Truong VK, Lapovok R, Estrin YS, Rundell S, Wang JY, Fluke CJ, et al. The influence of nano-scale surface roughness on bacterial adhesion to ultrafine-grained titanium. Biomaterials 2010;31:3674–83.
[293] Carman ML, Estes TG, Feinberg AW, Schumacher JF, Wilkerson W, Wilson LH, et al. Engineered antifouling microtopographies–correlating wettability with cell attachment. Biofouling 2006;22:11–21.
[294] Ma J, Sun Y, Gleichauf K, Lou J, Li Q. Nanostructure on taro leaves resists fouling by colloids and bacteria under submerged conditions. Langmuir 2011;27:10035–40.
[295] Rajab FH, Liauw CM, Benson PS, Li L, Whitehead KA. Production of hybrid macro/micro/nano surface structures on ti6al4v surfaces by picosecond laser surface texturing and their antifouling characteristics. Colloids Surf B Biointerfaces 2017;160: 688–96.
[296] Absolom DR, Lamberti FV, Policova Z, Zingg W, van Oss CJ, Neumann AW. Surface thermodynamics of bacterial adhesion. Appl Environ Microbiol 1983;46:90–7.
[297] Wan F, Ye Q, Yu B, Pei X, Zhou F. Multiscale hairy surfaces for nearly perfect marine antibiofouling. J Mater Chem B 2013;1:3599–606.
[298] Singh PK, Bartalomej S, Hartmann R, Jeckel H, Vidakovic L, Nadell CD, et al. Vibrio cholerae combines individual and collective sensing to trigger biofilm dispersal. Curr Biol 2017;27:3359–66.
[299] Muhammad MH, Idris AL, Fan X, Guo Y, Yu Y, Jin X, et al. Beyond risk: bacterial biofilms and their regulating approaches. Front Microbiol 2020;11.
[300] Korber DR, Lawrence JR, Lappin-Scott HM. Growth of microorganisms on. Microbial Biofilms 2003;5:15.
[301] Li G, Brown PJ, Tang JX, Xu J, Quardokus EM, Fuqua C, et al. Surface contact stimulates the just-in-time deployment of bacterial adhesins. Mol Microbiol 2012;83: 41–51.
[302] Wang L, Fan D, Chen W, Terentjev EM. Bacterial growth, detachment and cell size control on polyethylene terephthalate surfaces. Sci Rep 2015;5:15159.
[303] Gibiansky ML, Conrad JC, Jin F, Gordon VD, Motto DA, Mathewson MA, et al. Bacteria use type iv pili to walk upright and detach from surfaces. Science 2010;330:197.
[304] Gough N, Dodd C. The survival and disinfection of salmonella typhimurium on chopping board surfaces of wood and plastic. Food Control 1998;9:363–8.
[305] Whitehead KA, Verran J. The effect of surface topography on the retention of micro-organisms. Food Bioprod Process 2006;84:253–9.
[306] Bos R, Van der Mei HC, Busscher HJ. Physico-chemistry of initial microbial adhesive interactions–its mechanisms and methods for study. FEMS Microbiol Rev 1999;23: 179–230.
[307] Vilinska A, Rao KH. Surface thermodynamics and extended dlvo theory of leptospirillum ferrooxidans cells' adhesion on sulfide minerals. Min Metall Explor 2011;28:151–8.
[308] Masliyah JH, Bhattacharjee S. Electrokinetic and colloid transport phenomena. John Wiley & Sons; 2006.
[309] Spriano S, Chandra VS, Cochis A, Uberti F, Rimondini L, Bertone E, et al. How do wettability, zeta potential and hydroxylation degree affect the biological response of biomaterials? Mater Sci Eng C 2017;74:542–55.
[310] Wang L-L, Wang L-F, Ren X-M, Ye X-D, Li W-W, Yuan S-J, et al. Ph dependence of structure and surface properties of microbial eps. Environ Sci Technol 2012;46: 737–44.
[311] Van Oss C, Good R, Chaudhury M. Additive and nonadditive surface tension components and the interpretation of contact angles. Langmuir 1988;4:884–91.
[312] Israelachvili JN. Intermolecular and surface forces. Academic press; 2011.
[313] Probstein RF. Physicochemical hydrodynamics: An introduction. John Wiley & Sons; 2005.
[314] Israelachvili J, Pashley R. The hydrophobic interaction is long range, decaying exponentially with distance. Nature 1982;300:341–2.

[315] Feng G, Cheng Y, Wang S-Y, Hsu LC, Feliz Y, Borca-Tasciuc DA, et al. Alumina surfaces with nanoscale topography reduce attachment and biofilm formation by escherichia coli and listeria spp. Biofouling 2014;30:1253–68.
[316] Meinders J, Van der Mei H, Busscher H. Deposition efficiency and reversibility of bacterial adhesion under flow. J Colloid Interface Sci 1995;176:329–41.
[317] Van Oss C. Acid—base interfacial interactions in aqueous media. Colloids Surf A Physicochem Eng Asp 1993;78:1–49.
[318] Xu X, Jagota A, Hui C-Y. Effects of surface tension on the adhesive contact of a rigid sphere to a compliant substrate. Soft Matter 2014;10:4625–32.
[319] Maugis D. Contact, adhesion and rupture of elastic solids, volume 130; 2013 [Springer Science & Business Media].
[320] Long R, Shull KR, Hui C-Y. Large deformation adhesive contact mechanics of circular membranes with a flat rigid substrate. J Mech Phys Solids 2010;58:1225–42.
[321] Boks NP, Kaper HJ, Norde W, Busscher HJ, van der Mei HC. Residence time dependent desorption of staphylococcus epidermidis from hydrophobic and hydrophilic substrata. Colloids Surf B Biointerfaces 2008;67:276–8.
[322] Dąbroś T, Van de Ven T. Kinetics of coating by colloidal particles. J Colloid Interface Sci 1982;89:232–44.
[323] Boks NP, Busscher HJ, van der Mei HC, Norde W. Bond-strengthening in staphylococcal adhesion to hydrophilic and hydrophobic surfaces using atomic force microscopy. Langmuir 2008;24:12990–4.
[324] Kirbaşlar FG, Tavman A, Dülger B, Türker G. Antimicrobial activity of turkish citrus peel oils. Pak J Bot 2009;41:3207–12.
[325] Smith NM, Ebrahimi H, Ghosh R, Dickerson AK. High-speed microjets issue from bursting oil gland reservoirs of citrus fruit. Proc Natl Acad Sci 2018. https://doi.org/10.1073/pnas.1720809115 ISSN 0027-8424.
[326] Alam ME, Kauffman JL, Dickerson AK. Drop ejection from vibrating damped, dampened wings. Soft Matter 2020;16:1931–40.
[327] Dickerson AK, Hu DL. Mosquitoes actively remove drops deposited by fog and dew. Integr Comp Biol 2014:1–6.
[328] Dickerson A, Mills Z, Hu D. Wet mammals shake at tuned frequencies to dry. J R Soc Interface 2012;9:3208–18.
[329] Dickerson AK, Liu X, Zhu T, Hu DL. Fog spontaneously folds mosquito wings. Phys Fluids 2015;27:021901.
[330] Dickerson AK, Shankles PG, Madhavan NM, Hu DL. Mosquitoes survive raindrop collisions by virtue of their low mass. Proc Natl Acad Sci 2012;109:9822–7.
[331] Dickerson AK, Shankles PG, Hu DL. Raindrops push and splash flying insects. Phys Fluids 2014;26:027104.
[332] Bakken G. A heat transfer analysis of animals: unifying concepts and the application of metabolism chamber data to field ecology. J Theor Biol 1976;60:337–84.
[333] Gebremedhin K, Wu B. A model of evaporative cooling of wet skin surface and fur layer. J Therm Biol 2001;26:537–45.
[334] Ghosh R, Mukherjee S. Fully lagrangian modeling of dynamics of mems with thin beams—part i: undamped vibrations. J Appl Mech 2009:76.
[335] Ghosh R, Mukherjee S. Fully lagrangian modeling of dynamics of mems with thin beams—part ii: damped vibrations. J Appl Mech 2009:76.
[336] Ali H, Ebrahimi H, Ghosh R. Bending of biomimetic scale covered beams under discrete non-periodic engagement. Int J Solids Struct 2019;166:22–31.
[337] Ali H, Ebrahimi H, Ghosh R. Tailorable elasticity of cantilever using spatio-angular functionally graded biomimetic scales. Mech Soft Mater 2019;1:10.
[338] Ebrahimi H, Ali H, Horton RA, Galvez J, Gordon AP, Ghosh R. Tailorable twisting of biomimetic scale-covered substrate. EPL (Europhys Lett) 2019;127:24002.
[339] Ali H, Ebrahimi H, Ghosh R. Frictional damping from biomimetic scales. Sci Rep 2019;9:1–7.
[340] Ghosh R, Ebrahimi H, Vaziri A. Contact kinematics of biomimetic scales. Appl Phys Lett 2014;105:233701.
[341] Schumacher JF, Aldred N, Callow ME, Finlay JA, Callow JA, Clare AS, et al. Species-specific engineered antifouling topographies: correlations between the settlement of algal zoospores and barnacle cyprids. Biofouling 2007;23:307–17.
[342] Azeredo J, Azevedo NF, Briandet R, Cerca N, Coenye T, Costa AR, et al. Critical review on biofilm methods. Crit Rev Microbiol 2017;43:313–51.
[343] Christensen BB, Sternberg C, Andersen JB, Palmer Jr RJ, Nielsen AT, Givskov M, et al. [2] molecular tools for study of biofilm physiology. Methods in enzymology. Elsevier; 1999. p. 20–42.
[344] Heydorn A, Nielsen AT, Hentzer M, Sternberg C, Givskov M, Ersbøll BK, et al. Quantification of biofilm structures by the novel computer program comstat. Microbiology 2000;146:2395–407.
[345] Percival S, Knapp J, Wales D, Edyvean R. The effect of turbulent flow and surface roughness on biofilm formation in drinking water. J Ind Microbiol Biotechnol 1999;22:152–9.
[346] Hornemann JA, Codd SL, Fell RJ, Stewart PS, Seymour JD. Secondary flow mixing due to biofilm growth in capillaries of varying dimensions. Biotechnol Bioeng 2009;103:353–60.
[347] Halder P, Nasabi M, Jayasuriya N, Shimeta J, Deighton M, Bhattacharya S, et al. An assessment of the dynamic stability of microorganisms on patterned surfaces in relation to biofouling control. Biofouling 2014;30:695–707.
[348] Suwarno SR, Huang W, Chew YJ, Tan SHH, Trisno AE, Zhou Y. On-line biofilm strength detection in cross-flow membrane filtration systems. Biofouling 2018;34:123–31.
[349] Aufrecht JA, Fowlkes JD, Bible AN, Morrell-Falvey J, Doktycz MJ, Retterer ST. Pore-scale hydrodynamics influence the spatial evolution of bacterial biofilms in a microfluidic porous network. PLoS One 2019;14:e0218316.
[350] Griebe T, Flemming H-C. Rotating annular reactors for controlled growth of biofilms. Lancaster, PA: Technomic Publishing Co, Inc.; 2000.
[351] Mukherjee M, Menon NV, Liu X, Kang Y, Cao B. Confocal laser scanning microscopy-compatible microfluidic membrane flow cell as a nondestructive tool for studying biofouling dynamics on forward osmosis membranes. Environ Sci Technol Lett 2016;3:303–9.
[352] Rath H, Stumpp SN, Stiesch M. Development of a flow chamber system for the reproducible in vitro analysis of biofilm formation on implant materials. PLoS One 2017;12:e0172095.
[353] Nolte KA, Schwarze J, Rosenhahn A. Microfluidic accumulation assay probes attachment of biofilm forming diatom cells. Biofouling 2017;33:531–43.
[354] Duckworth PF, Rowlands RS, Barbour ME, Maddocks SE. A novel flow-system to establish experimental biofilms for modelling chronic wound infection and testing the efficacy of wound dressings. Microbiol Res 2018;215:141–7.
[355] Nolte KA, Schwarze J, Beyer CD, Özcan O, Rosenhahn A. Parallelized microfluidic diatom accumulation assay to test fouling-release coatings. Biointerphases 2018;13:041007.
[356] Zhang Y, Li C, Wu Y, Zhang Y, Zhou Z, Cao B. A microfluidic gradient mixer-flow chamber as a new tool to study biofilm development under defined solute gradients. Biotechnol Bioeng 2019;116:54–64.
[357] White-Ziegler CA, Malhowski AJ, Young S. Human body temperature (37 c) increases the expression of iron, carbohydrate, and amino acid utilization genes in escherichia coli k-12. J Bacteriol 2007;189:5429–40.
[358] Wei Y, Murphy ER. Temperature-dependent regulation of bacterial gene expression by rna thermometers. Nucleic Acids-From Basic Asp Lab Tools 2016;157.
[359] Lo M, Bulach DM, Powell DR, Haake DA, Matsunaga J, Paustian ML, et al. Effects of temperature on gene expression patterns in leptospira interrogans serovar lai as assessed by whole-genome microarrays. Infect Immun 2006;74:5848–59.
[360] Liles MR, Viswanathan V, Cianciotto NP. Identification and temperature regulation oflegionella pneumophila genes involved in type iv pilus biogenesis and type ii protein secretion. Infect Immun 1998;66:1776–82.
[361] Ramia M, Tullock D, Phan-Thien N. The role of hydrodynamic interaction in the locomotion of microorganisms. Biophys J 1993;65:755–78.
[362] Wadowsky RM, Wolford R, McNamara A, Yee RB. Effect of temperature, ph, and oxygen level on the multiplication of naturally occurring legionella pneumophila in potable water. Appl Environ Microbiol 1985;49:1197–205.
[363] Gonthier A, Guérin-Faublée V, Tilly B, Delignette-Muller M-L. Optimal growth temperature of o157 and non-o157 escherichia coli strains. Lett Appl Microbiol 2001;33:352–6.
[364] Ratkowsky DA, Olley J, McMeekin T, Ball A. Relationship between temperature and growth rate of bacterial cultures. J Bacteriol 1982;149:1–5.
[365] Pavlovsky L, Younger JG, Solomon MJ. In situ rheology of staphylococcus epidermidis bacterial biofilms. Soft Matter 2013;9:122–31.
[366] Gu H, Lee SW, Buffington SL, Henderson JH, Ren D. On-demand removal of bacterial biofilms via shape memory activation. ACS Appl Mater Interfaces 2016;8:21140–4.
[367] Pavlovsky L. Novel methods for rheological characterization of polymers and polymeric biofilms. Ph.D. thesis; 2014.
[368] Harvey, J. Chamberland, charles edouard. eLS.
[369] Costerton JW, Cheng K, Geesey GG, Ladd TI, Nickel JC, Dasgupta M, et al. Bacterial biofilms in nature and disease. Annu Rev Microbiol 1987;41:435–64.
[370] Gorur A, Lyle DM, Schaudinn C, Costerton JW. Biofilm removal with a dental water jet. Compendium of continuing education in dentistry (Jamesburg, NJ: 1995), 30. ; 2009. p. 1–6.
[371] Sahni K, Khashai F, Forghany A, Krasieva T, Wilder-Smith P. Exploring mechanisms of biofilm removal. Dentistry (Sunnyvale, Calif) 2016;6.
[372] Bao P, Shen Y, Lin J, Haapasalo M. In vitro efficacy of xp-endo finisher with 2 different protocols on biofilm removal from apical root canals. J Endod 2017;43:321–5.
[373] Ordinola-Zapata R, Bramante C, Aprecio R, Handysides R, Jaramillo D. Biofilm removal by 6% sodium hypochlorite activated by different irrigation techniques. Int Endod J 2014;47:659–66.
[374] Jennings W, McKillop A, Luick J. Circulation cleaning. J Dairy Sci 1957;40:1471–9.
[375] Powell MS, Slater NK. Removal rates of bacterial cells from glass surfaces by fluid shear. Biotechnol Bioeng 1982;24:2527–37.
[376] Van Bel N, Hornstra LM, Van Der Veen A, Medema G. Efficacy of flushing and chlorination in removing microorganisms from a pilot drinking water distribution system. Water 2019;11:903.
[377] Bott T. Techniques for reducing the amount of biocide necessary to counteract the effects of biofilm growth in cooling water systems. Appl Therm Eng 1998;18:1059–66.
[378] Salta M, Goodes L, Maas B, Dennington S, Secker T, Leighton T. Bubbles versus biofilms: a novel method for the removal of marine biofilms attached on antifouling coatings using an ultrasonically activated water stream. Surf Topogr Metrol Prop 2016;4:034009.